finding suggests that the mechanism of pathogenesis is derived from aggregation of proteins or peptides with the expanded polyQ. By contrast, the onset of a neurological phenotype or cell dysfunction mediated by the expanded polyQ in the responsible gene product was independent of the formation of inclusions [5–7]. Indeed, a previous study showed that the presence of inclusion bodies reduced the risk of neuronal death as a result of polyQ expansion [8]. Thus, the relationship between inclusions and neurotoxicity remains controversial [9]. The polyQ diseases show progressive and refractory neurological symptoms that are caused by neuronal cell loss in selective regions of the central nervous system. This selective neuronal damage gives rise to the specific features of each disease. Accordingly, we hypothesized that each polyQ disease has a distinct molecular mechanism underlying its characteristic neurodegeneration.

DRPLA is an autosomal dominant neurodegenerative disorder characterized clinically by progressive dementia, epilepsy, gait disturbance and involuntary movement (chorea and myoclonus) and, pathologically, by combined degeneration of the dentatorubral and pallidoluysian systems [10,11]. DRPLA pedigrees show genetic anticipation and phenotypic heterogeneity [12–14]. DRPLA is caused by expansion of the polyQ tract within DRPLA protein, also known as atrophin-1 (ATN1). ATN1 is ubiquitously expressed in the central nervous system, although selective regions of the central nervous system are involved in the neuronal degeneration in DRPLA [15]. A previous study using cultured cells expressing ATN1 showed that truncated ATN1 with an expanded polyQ formed perinuclear and intranuclear aggregates and caused apoptotic cell death [16]. Cleavage of ATN1 may be relevant to the disease pathogenesis, although the nature of the relevant cleavage product is uncertain. Previous studies in a transgenic mice model and DRPLA patients have shown that a 120 kDa N-terminal fragment of mutant ATN1 accumulates within the nuclei of neurones [17,18]. On the other hand, we have previously reported evidence of an ∼ 100 kDa C-terminal fragment in the normal control and DRPLA human brains [15]. Caspase cleavage of ATN1 at Asp109 generates a large C-terminal fragment [19–21], although whether the caspase cleavage occurs *in vivo* remains uncertain. In the present study, we report a novel C-terminal fragment of ATN1 that contains a polyQ tract found in cellular models of DRPLA, which expresses ATN1 and manifests accumulation of ATN1 with the expanded polyQ. Moreover, the novel C-terminal fragment with the expanded polyQ was discovered in the brain tissues of DRPLA patients. From these results,

we hypothesize that pathological ATN1 accumulation underlies neurodegeneration in DRPLA.

Results

Construction of shortened and expanded CAG repeat of *ATN1* gene

The *ATN1* gene was fused to a His-tag and a T7-tag at the 5′-end, and to a *Strep*-tag II at the 3′-end (Fig. 1A). To produce mutant proteins with various numbers of glutamine repeats, we established a method for making the intended CAG repeat a stable PCR product. PCR was performed using oligonucleotides, 5′-(CAG)$_{10}$-3′ and its complementary strand, without DNA templates. The approximately required size of the CAG repeat was obtained by PCR with CAG/CTG oligomer (Fig. S1). The full-length mutant *ATN1* genes were prepared by cassette mutagenesis. The full-length cDNAs of ATN1 with different numbers of the CAG repeat were constructed; the numbers of the translated glutamine repeat are 0, 4, 19, 31, 47, 54 and 77 (Fig. 1B). The polyQ repeat size 0 is a deletion, 4 is shortened, 19 and 31 are normal, 47 is borderline, and 54 and 77 are in the abnormal range. Each expressed protein was represented by adding the number of glutamine repeats it includes after ATN1 (e.g. ATN1-Q19).

Expression of ATN1 in mammalian cells

The cloned cDNA of ATN1 encoded a 1190 amino acid protein that contains the normal 19 polyQ repeat (ATN1-Q19). ATN1 expression systems were constructed for COS-7 and Neuro2a cells. COS-7 and Neuro2a cells were transiently transfected with *ATN1-Q19*-pcDNA3.1 by lipofection. We detected cellular expression of ATN1s with ATN1 antibodies: L55-2 and C580R. Immunoblots of ATN1-Q19 expressed in COS-7 and Neuro2a cells revealed that the ATN1 antibodies labelled two C-terminal fragments of ATN1 with estimated molecular masses of 140 kDa (F1) and 125 kDa (F2), in addition to the full-length ATN1 (Figs 1C,D and S2). The T7-tag antibody detected only the full-length ATN1 at 165 kDa but no fragment (Fig. 1C). Immunoblots of ATN1-Q77 in COS-7 and Neuro2a cells also revealed that L55-2 and C580R recognized the full-length ATN1 at 185 kDa and two C-terminal fragments (Fig. 1C,D). These 160 and 145 kDa fragments corresponded with the mutant F1 fragment with expanded polyQ (mF1) and the mutant F2 fragment (mF2), respectively. The immunoblots of ATN1-Q19 and -Q77 also showed that an antibody

146
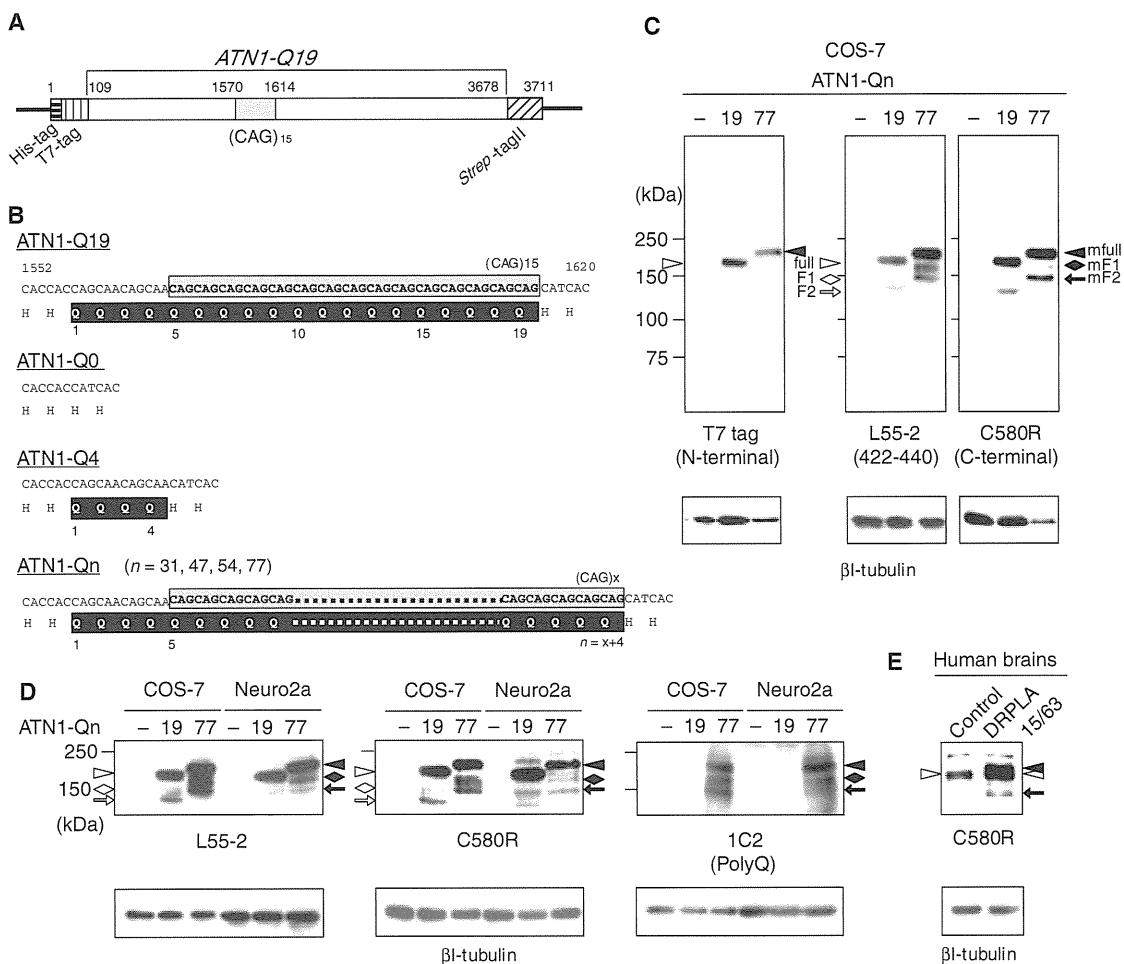
Fig. 1. (A) cDNA constructs of *ATN1* gene and expression of ATN1 in mammalian cells. The ORF of *ATN1-Q19* is shown in the box. The regions encoding the three tags are hatched and the CAG repeat is shown in grey. Numbers above the box represent the positions of the nucleotide counted from the initiation of the cDNA construct. (B) A series of polyQ regions of mutated ATN1 are illustrated. The nucleotides and their corresponding amino acid sequences around the CAG repeat are shown. The regions of CAG repeat in cDNA are shown in grey and the polyQ in the amino acid sequences is shown in black. (C) ATN1-Q19 and -Q77 were expressed in COS-7 cells. Expressed ATN1 was detected by immunoblotting using T7-tag, L55-2 and C580R antibodies. The immunoblots revealed that the full-length ATN1 was cleaved into two fragments containing the C-terminal and polyQ tract. The arrowheads show the full-length ATN1-Q19 (white) and full-length ATN1-Q77 (black). C-terminal fragments are defined as F1 (white lozenge) and F2 (white arrow). In ATN1-Q77, they are defined as mF1 (black lozenge) and mF2 (black arrow). βI-tubulin was examined as a loading control. (D) We expressed ATN1-Q19 and -Q77 in COS-7 and Neuro2a cells. ATN1s expression was compared using immunoblotting with ATN1 antibodies (C580R and L55-2) and polyQ antibody (1C2). The antibodies showed no difference in immunoreactivity of ATN1 and various fragments between the Neuro2a and COS-7 cells. 1C2 labelled the ATN1-Q77 bands but not the ATN1-Q19 band. βI-Tubulin was used as a loading control. Representative immunoblots of three independent experiments are shown. (E) Tissue samples of the cerebellum of a patient with DRPLA and the human control brain tissue were examined by immunoblotting. The antibody C580R recognized the C-terminal of ATN1 mutant (black arrowhead) and wild-type (white arrowhead), the full-length ATN1s in the DRPLA brain tissue. A novel C-terminal fragment mF2 with an expanded polyQ tract (black arrow) was identified in the DRPLA brain tissue.

against polyQ tracts, 1C2, detected the same immunoreactivity of ATN1 and fragments as L55-2 (Fig. 1D), which indicates that the C-terminal fragments of mF1 and mF2 contained polyQ tracts.

Furthermore, the brain tissues from DRPLA patients also contained the C-terminal fragment of ATN1 containing an expanded polyQ tract. Immunoblots of

the brain tissues from DRPLA patients revealed an immunoreactive, C580R-labelled band at ~ 150 kDa, which corresponds with the results of mF2 fragment of ATN1-Q77 in COS-7 cells (Fig. 1E, black arrow). Taken together, these results demonstrated that the mutant, full-length ATN1 was cleaved into the C-terminal fragment of mF2 in the mammalian cultured cells and

human brains. Because immunoblots revealed apparently different amounts of the full-length ATN1 and C-terminal fragment proteins in ATN1-Q19 and -Q77 of the COS-7 expression, we performed a quantitative assessment of ATN1 expression by western blotting with *Strep*-Tactin horseradish peroxidase (HRP) conjugate.

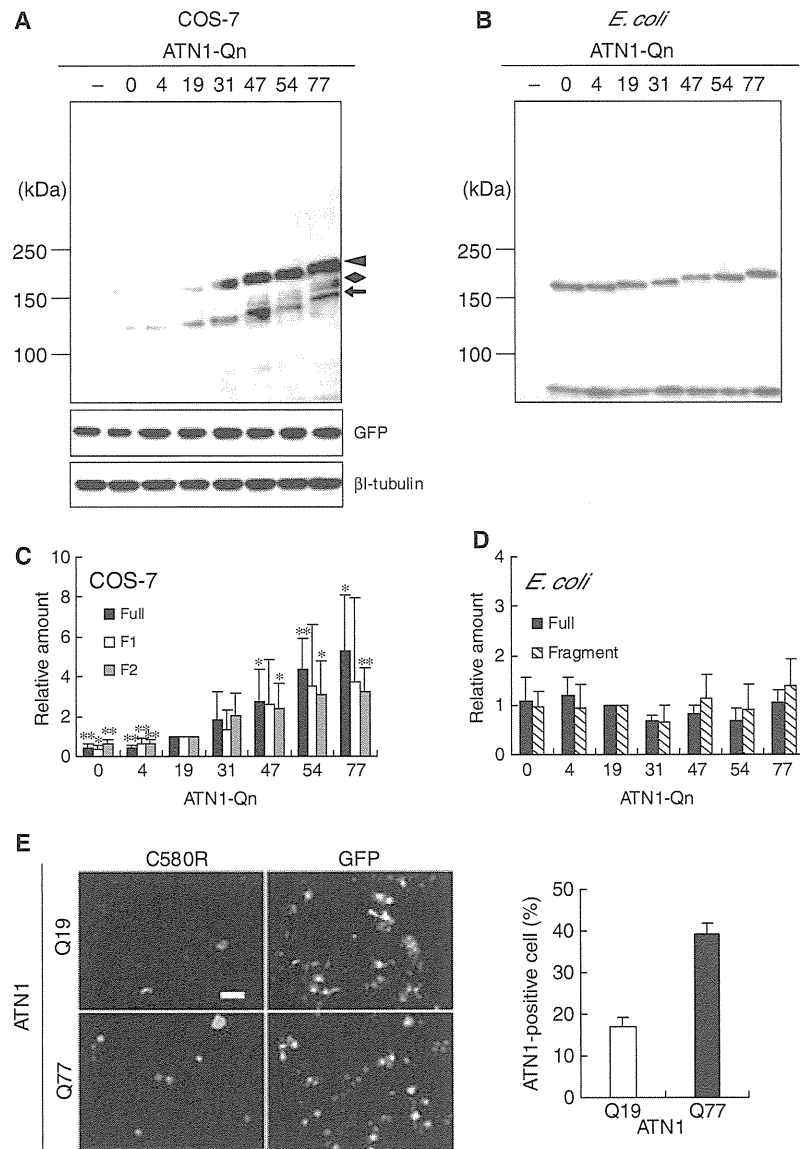## Accumulation of ATN1 and C-terminal fragments with expansion of polyQ in COS-7 cells

To examine differential expression of ATN1 with varying numbers of polyQs, ATN1-Q0, -Q4, -Q19, -Q31, -Q47, -Q54 and -Q77 were overexpressed in COS-7 cells and *Escherichia coli*. We directly detected ATN1s with *Strep*-tag II expressed in the COS-7 cells and *E. coli* using western blotting with the *Strep*-Tactin HRP conjugate. Western blots of the expressed ATN1s in COS-7 cells showed that the reactivity of the full-length ATN1 and F2 bands increased with the increase of the polyQ size (Fig. 2A), whereas the blots of ATN1s in *E. coli* showed no difference in the reactivity of the full-length or fragmented ATN1s (Fig. 2B). Quantitative analyses of the blots confirmed the increased reactivity in COS-7 cells but not in *E. coli* (Fig. 2C,D). In addition, an immunocytochemical study of COS-7 cells expressing ATN1s showed an apparent increase in the immunoreactivity of ATN1 antibody with ATN1-Q77 compared to ATN1-Q19 (Fig. 2E). These data indicate that the amount of the full-length ATN1 and fragments increased in the COS-7 cells as the size of the polyQ was increased.

Next, we assessed whether the quantitative increase of the full-length ATN1 and fragments was the result of an accumulation caused by the prolonged life span of the proteins. We examined the stability of ATN1-Q19 and -Q77 by inhibition of protein synthesis. At each time point, equal amounts of protein were separated in gels, and these were examined by western blotting. We found that, after cycloheximide treatment, the protein levels of ATN1 and fragments were quickly decreased by degradation, whereas no reduction of βI-tubulin or green fluorescent protein (GFP) (controls) occurred (Fig. 3A). ATN1-Q77 and -Q19 exhibited significantly different speeds of degradation. Western blots showed that the full-length ATN1 decreased to $\sim 70\%$ at 30 min after treating ATN1-Q77 with cycloheximide, whereas the full-length ATN1-Q19 decreased to $< 20\%$ at 30 min (Fig. 3B). These results indicate the increase of ATN1 and fragments was a result of accumulation. Moreover, the mF2 fragment showed a smaller decrease than the mutant, full-length ATN1 and mF1 fragment in ATN1-Q77 at 30 min after treatment (Fig. 3C). Thus,

the mF2 fragment is selectively accumulated by the expansion of the polyQ tract. We then investigated where mF2 accumulated in the cells.

Subcellular localization of ATN1 and fragments

Although previous immunohistological studies showed that ATN1 localized to both the nucleus and cytoplasm of neuronal cells [15,22,23], the precise intracellular localization of the ATN1 fragments remains unclear. To determine the intracellular localization of the full-length ATN1 and the C-terminal fragments, we first biochemically analyzed COS-7 cells that expressed ATN1 by subcellular fractionation using low-speed centrifugation. The COS-7 cells were fractionated into crude nuclear and non-nuclear fractions. Western blots of COS-7 expressing ATN1-Q19 revealed that the full-length ATN1 was located in the nuclear and non-nuclear fractions, although the C-terminal fragments were located only in the nuclear fraction (Fig. S3). Furthermore, western blots of COS-7 cells expressing ATN1-Q77 showed that the full-length ATN1 and the mF2 fragment were located in the nuclear and non-nuclear fractions. To further elucidate the intracellular localization of the full-length ATN1 and fragments, we performed subcellular fractionation of the proteins into four fractions: cytosol, cytoplasmic membrane/organelle, nucleus and insoluble. Western blots of ATN1-Q19 displayed reactivity of the full-length ATN1 and F2 in both the nuclear and insoluble fractions but F1 in the insoluble fraction only (Fig. 4A). Furthermore, western blots of ATN1-Q77 indicated mF2 was located in the membrane/organelle and insoluble fractions, in addition to the nuclear fraction (Fig. 4A). The mutant, full-length ATN1 and mF1 of ATN1-Q77 were observed in the same fractions as those of ATN1-Q19. The blotting data indicated that the F2 fragment was located in the nuclear and insoluble fractions of those ATN1s with a normal polyQ repeat size, whereas mF2 showed specific localization in the cytoplasmic membrane/organelle fraction in addition to the other fractions when the size of the polyQ tract was expanded. We immunocytochemically examined the COS-7 cells 24 h after transfection using His-tag antibody and C580R. Both antibodies showed diffuse nuclear staining and granular cytoplasmic staining (Fig. 4B). The ATN1-Q19 and -Q77 exhibited similar localization in the cytoplasm and nucleus. However, the immunoreactivity of ATN1-Q77 was stronger than that of ATN1-Q19. Taken together, these biochemical and immunocytochemical studies revealed that the full-length ATN1 and the fragments localized in the nucleus and in the cytoplasm, and that

Fig. 2. Accumulation of ATN1 and fragments as a result of expanded polyQ in COS-7 cells. (A) Transiently expressed ATN1-Q0, -Q4, -Q19, -Q31, -Q47, -Q54 and -Q77 in COS-7 cells were examined by western blotting using *Strep*-Tactin HRP conjugate. Western blots showed that the reactivity of the full-length ATN1, F1 and F2 increased with the increase of polyQ size. GFP was used as a transfection control and βI-tubulin as a loading control. The arrowhead, lozenge and arrow indicate the full-length ATN1, F1 and F2, respectively. (B) ATN1s were expressed in *E. coli* Rosetta(DE3)pLysS. Western blotting showed no changes in the reactivity of the full-length ATN1 and C-terminal fragments with any polyQ size. (C) Quantification is presented as the relative ratio of the full-length ATN1 (black), F1 (white) and F2 (grey) to βI-tubulin in COS-7 cells. Densitometric measurement of the signals was performed using IMAGEJ software (US National Institutes of Health, Bethesda, MD, USA) and the intensities of the signals were expressed as relative values. The density is relative to each ATN1-Q19 peptide as the corresponding control. These data showed that the full-length ATN1 and F2 expression increased with the increase of polyQ size in COS-7 cells. $*P < 0.05$ and $**P < 0.01$ (Student's t-tests). The height of the columns indicates the relative amount and the error bars represent the SD ($n = 5$). (D) Relative quantification of signals of the full-length ATN1 (black) and a C-terminal fragment (stripe) of ATN1 from bacterial cells. Densitometric measurement of the signals showed that there was no quantitative difference among the ATN1s and fragments expressed in *E. coli* with any polyQ size. The density is relative to the full-length ATN1-Q19 protein as the control. The height of the columns indicates the relative amount and the error bars represent the SD ($n = 3$). (E) Twenty-four hours after transfection with the ATN1-Q19 or -Q77 construct, COS-7 cells were immunostained with ATN1 antibody C580R (left panels) or GFP antibody (right panels). C580R detected more ATN1 immunoreactivity in ATN1-Q77 than in ATN1-Q19, whereas GFP showed no significant difference between constructs. Scale bar = 100 μm. The bar graph shows the ratio of ATN1-positive cells to co-expressed GFP-positive cells, and error bars represent the SD ($n = 3$).
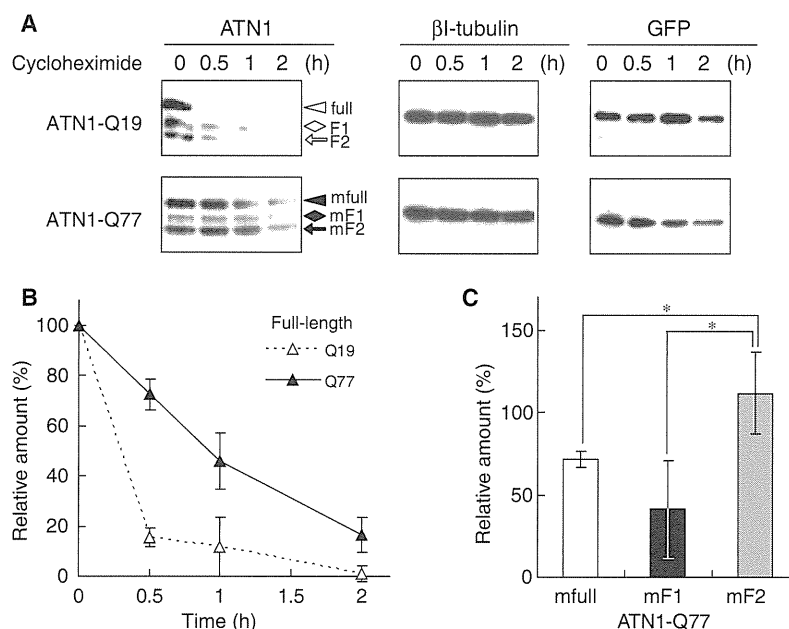
Fig. 3. Effect of polyQ size on stability of ATN1 peptides. (A) COS-7 cells transfected ATN1-Q19 and -Q77 were treated with 100 μg·mL^{-1} cycloheximide (at time 0), which blocks protein synthesis in eukaryotic cells. At the indicated time points, the cells were harvested as described in the Experimental procedures. Western blots showed that the full-length ATN1s and fragments were quickly decreased over time. (B) At all time points, the full-length ATN1-Q19 and -Q77 were quantitatively assessed on the western blots. The line graph shows that ATN1-Q77 was degraded more slowly than ATN1-Q19 in the cells. $*P < 0.05$ (Student's t-test). The points indicate the relative amount and the error bars represent the SD ($n = 3$). (C) Thirty minutes after treatment of ATN1-Q77, the mutant full-length, mF1 and mF2 levels were quantitatively assessed on the blots. The bar graph shows that the decrease in mF2 was less than those in the full-length ATN1 and mF1. Means data are plotted from four independent experiments. $*P < 0.05$ (Student's t-test). Error bars represent the SD.

the mF2 fragment with an expanded polyQ tract also localized in the membrane/organelle and insoluble fractions of the cytoplasm. Thus, expansion of the polyQ tract induces pathological accumulation of the mF2 fragment of ATN1 in the cytoplasm.

Furthermore, to explore the biological relevance of polyQ expansion in the ATN1s to cell toxicity, we performed terminal deoxynucleotidyl transferase-mediated dUTP nick end labelling (TUNEL) assays to detect nuclear fragmentation, which is a hallmark of apoptosis. TUNEL-staining showed that expression of ATN1-Q77 in Neuro2a cells induced apoptosis, whereas the expression of ATN1-Q19 resulted in no apoptosis (Fig. S4). These data suggest that ATN1 and fragments with expanded polyQ could cause neurotoxicity by the accumulation of mF2 in the cytoplasmic membrane/organelle fraction.

Cleavage of ATN1 into mF2 in the brain tissues of DRPLA patients

We next assessed the proteolytic processing of ATN1 in the brain tissue of DRPLA patients and compared it with that of recombinant ATN1 in COS-7 cells. We

examined, postmortem, the brain tissues from a DRPLA patient whose DRPLA genes contained 63 and 15 CAG repeats. Total homogenate and a crude nuclear fraction were prepared from the DRPLA brain tissues, and were then examined by immunoblotting with C580R. Immunoblots of the total homogenate and the nuclear fraction showed an immunoreactive band at ~ 140 kDa that corresponded to mF2 in COS-7 cells in addition to the mutant and wild-type, full-length ATN1s (Fig. 5A). Next, we examined the intracellular localization of ATN1 using the subcellular fractionation of the protein into the four fractions as described above. The mF2 fragment in the cerebellum of the DRPLA brain was demonstrated in the cytoplasmic membrane/organelle and insoluble fractions on the immunoblots by staining with C580R, L55-2 and 1C2 antibodies (Fig. 5B). We observed a single immunoreactive band of mF2 with an expanded polyQ but no other immunoreactive band for F2 with a normal sized polyQ from the DRPLA brain tissue. Using immunohistochemical staining with the ATN1 antibody, we noticed L55-2 labelled neuronal intranuclear and cytoplasmic inclusions in the affected lesion of the DRPLA brain tissues (Fig. 5C).
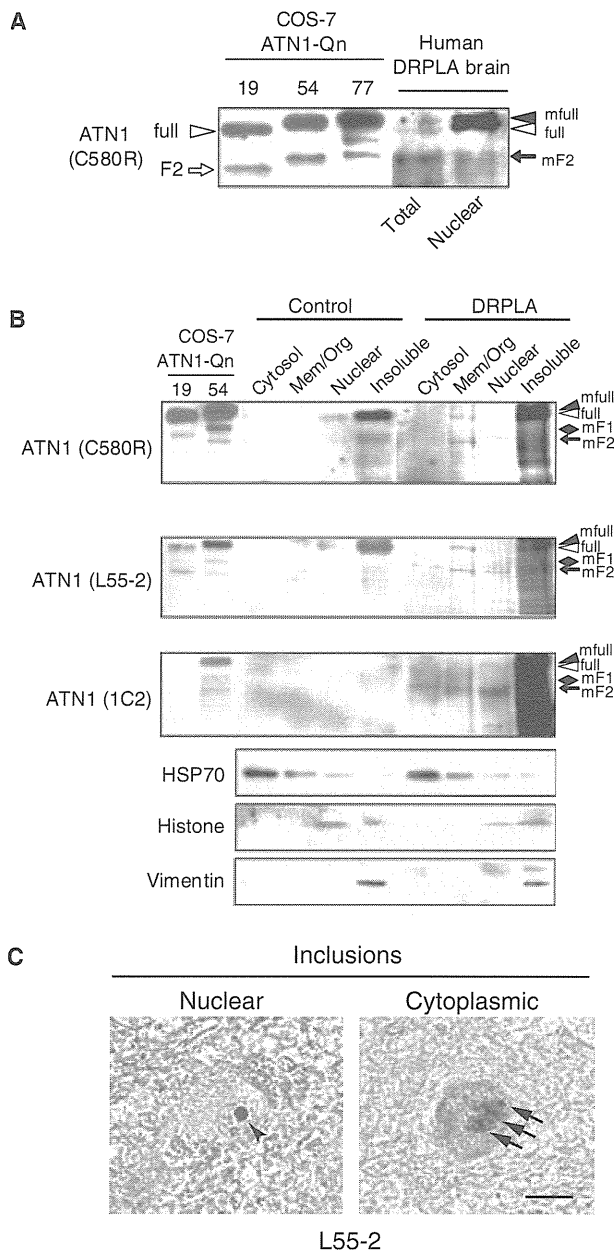
Fig. 4. Subcellular localization of ATN1-Q19 and -Q77 expressed in COS-7 cells. (A) After 48 h of transfection, the expressed cells were fractionated into cytosolic, membrane/organelle (Mem/Org), nuclear and insoluble fractions, in accordance with the protocol of the ProteoExtract subcellular proteome extraction kit. Western blotting showed that the full-length ATN1s (arrowheads) were detected in the nuclear and insoluble fractions, whereas F1 and mF1 were detected in the insoluble fraction (lozenges). Note that mF2 is found in the membrane/organelle, nuclear and insoluble fractions (black arrow). Stacked bar graphs present the ratio of distribution of F2 and mF2. Data are plotted from four independent experiments. *P < 0.05 (Student's t-test). To display the selectivity of subcellular fractions, marker proteins were immunoblotted with three antibodies: HSP70 for cytosolic, TFIID for nuclear and vimentin for insoluble fractions. Ten micrograms of protein were loaded per lane. Representative immunoblots of four independent experiments are shown. (B) Twenty-four hours after transfection with the ATN1-Q19 or -Q77 construct, COS-7 cells were visualized by immunofluorescence microscopy. Immunocytochemistry using His-tag (green) and C580R (red) antibodies shows that ATN1-Q19 and -Q77 were localized both in the cytoplasm and nucleus. The immunoreactivity of ATN1-Q77 was stronger than that of ATN1-Q19. Scale bar = 10 μm.
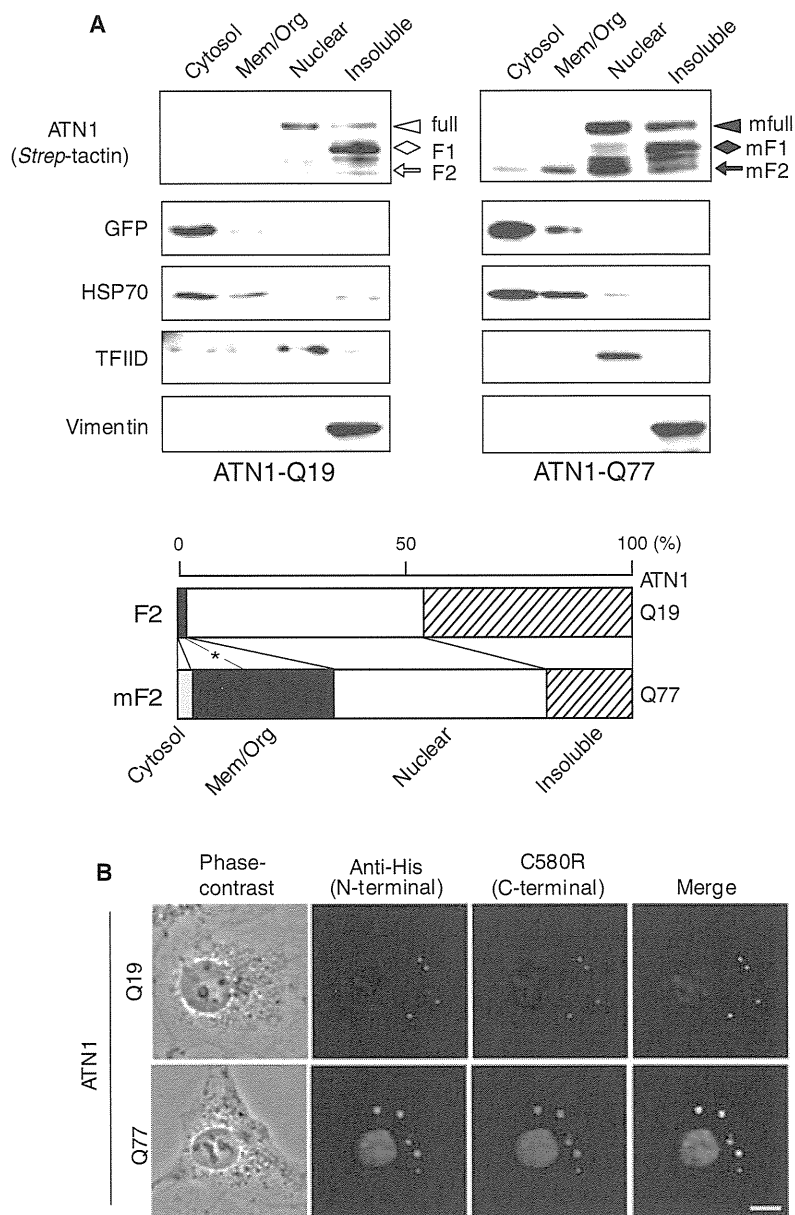
Accumulation of F2 is increased by inhibition of caspase

To clarify the proteolytic processing of ATN1 and understand its regulation, we treated the ATN1-expressing COS-7 cells with protease inhibitors, including caspase inhibitors, and assessed the resultant cell lysates by western blotting. When cells expressing ATN1-Q19 were treated with proteasome inhibitors, the blotting analysis showed that the amounts of the full-length ATN1 and F1 increased (Fig. 6A). Specific inhibitors of proteasomes (MG-132 and lactacystin)

and a nonspecific inhibitor [N-acetyl-Leu-Leu-norleucinal (ALLN) at 20 μM] increased the full-length ATN1, although ALLN did not affect ATN1 at 0.2 μM. These findings indicate that the ubiquitin-proteasome pathway is involved in the processing of ATN1, and the proteasome appears to primarily target the full-length ATN1. By contrast, when the cells were treated with caspase inhibitors, the blot membrane showed that the full-length ATN1 and F2 were increased by treatment with a pan-caspase inhibitor, benzyloxycarbonyl-Val-Ala-Asp(OMe)-fluoromethyl ketone (Z-VAD-FMK), although they were not increased by other selective
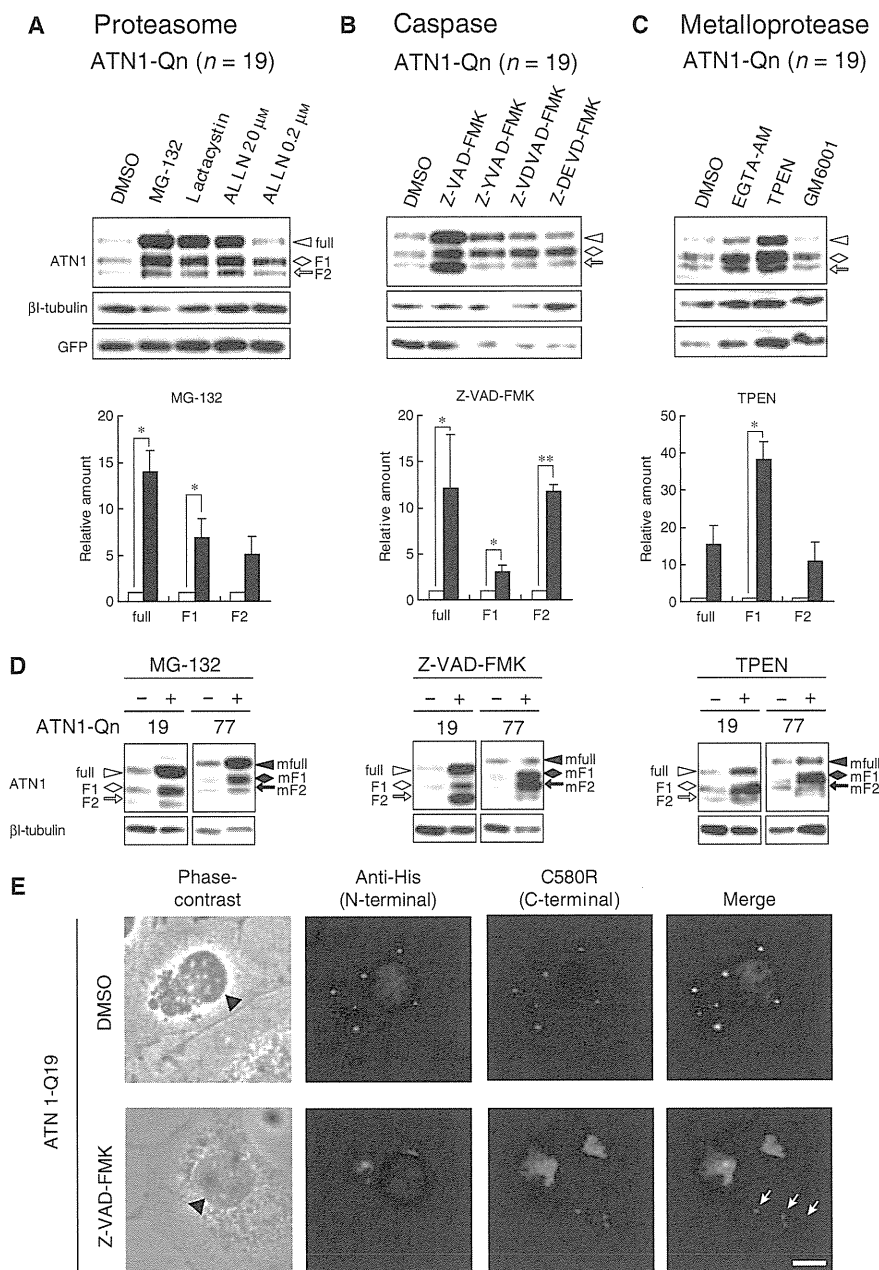
151

A

B

C

Inclusions

L55-2

Fig. 5. Subcellular localization of ATN1 in the human DRPLA brain tissues. (A) Samples of COS-7 cells expressing ATN1-Q19, -Q54 and -Q77, and the cerebellum of a DRPLA patient were immunoblotted using C580R. Because the DRPLA patient had 63 and 15 CAG repeats on the DRPLA gene, ATN1-Q19, -Q54 and -Q77, were useful for comparison. The immunoblot showed that a single band of the mF2 fragment with expanded polyQ was specifically found in the DRPLA brain tissue (black arrow). (B) The human control and DRPLA brain tissues were fractionated into cytosolic, cytoplasmic membrane/organelle (Mem/Org), nuclear and insoluble fractions. To display the selectivity of subcellular fractions, marker proteins were immunoblotted with three antibodies: HSP70 for cytosolic, Histone H4 for nuclear and vimentin for insoluble fractions. ATN1 (C580R and L55-2) and polyQ antibodies detected the immunoreactivity of mF2 in the cytoplasmic membrane/organelle and insoluble fractions of the DRPLA brain tissues. Twenty micrograms of protein were loaded per lane. Representative immunoblots of three independent experiments are shown. (C) The brain tissues of the DRPLA patient were immunohistochemically stained with L55-2. L55-2-labelled neuronal nuclear (arrowhead) and cytoplasmic inclusions (arrows) in the dentate nucleus. Scale bar = 10 μm.

other protease inhibitors showed no increase of these bands (Fig. S5B). Although proteasome inhibitors and the zinc-dependent protease inhibitor were involved in the accumulation of the full-length ATN1 and F1, Z-VAD-FMK selectively induced the accumulation of the full-length ATN1 and F2 in COS-7 cells.

To investigate the effect of polyQ expansion on the proteolytic processing of ATN1, we also examined COS-7 cells expressing ATN1 with normal and expanded polyQ tract after treatment with protease inhibitors. Western blots containing cells treated with Z-VAD-FMK revealed that mF2 in ATN1-Q77 with treatment of Z-VAD-FMK displayed higher reactivity than that without the treatment, whereas the full-length ATN1 in ATN1-Q77 showed similar reactivity with and without the treatment (Figs 6D and S5A). These data indicated that polyQ expansion induced the accumulation of mF2 by inhibition of caspases. We further investigated how Z-VAD-FMK treatment influenced the subcellular distribution of ATN1 and its fragments, by performing immunocytochemical analysis to compare untreated and Z-VAD-FMK-treated cells. Cells treated with Z-VAD-FMK showed that the aggregation composed by the C-terminal fragments of ATN1 increased in the cytoplasm (Fig. 6E). Moreover, Z-VAD-FMK treatment decreased immunoreactivity in the nucleus, demonstrating a difference compared to cells expressing ATN1-Q77.

Discussion

One of the primary pathological processes underlying the neurodegeneration that occurs in DRPLA is

caspase inhibitors (Fig. 6B). COS-7 cells expressing ATN1 were also treated with metalloprotease inhibitors. The blots of cell lysates treated with N,N,N′,N′-tetrakis(2-pyridylmethyl)ethylenediamine (TPEN) showed an increase in the full-length ATN1 and F1, although those treated by other metalloprotease inhibitors showed no increase (Fig. 6C). When COS-7 cells expressing ATN1 were subjected to double treatment with two inhibitors, Z-VAD-FMK and TPEN, the blot showed that both F1 and F2 increased (Fig. S5A). Z-VAD-FMK selectively increased the signal intensity of F2. Thus, F1 and F2 were processed in different pathways. Western blots including cells treated with

152

Fig. 6. Effect of protease inhibitors on ATN1-Q19 and -Q77 expressed in COS-7 cells. After 24 h of transfection, COS-7 cells expressing ATN1-Q19 were incubated for 24 h in serum-free medium with inhibitors: (A) proteasome and calpain inhibitors, MG-132 (10 μM), lactacystin (25 μM) and ALLN (20 μM, 0.2 μM); (B) caspase inhibitors, Z-VAD-FMK (50 μM for pan caspase), Z-YVAD-FMK (50 μM for caspase-1/4), Z-VDVAD-FMK (50 μM for caspase-2) and Z-DEVD-FMK (50 μM for caspase-3/6/7/10); and (C) metalloprotease inhibitors, EGTA-AM (50 μM for Ca^{2+}-dependent protease), TPEN (0.5 μM for Zn^{2+}-dependent protease) and GM6001 (50 μM for matrix metalloprotease). Western blotting showed that the reactivity of the C-terminal F2 fragment (white arrow) was increased by Z-VAD-FMK but was not significantly increased by the other inhibitors. Bar graphs include a quantitative analysis of ATN1s on the blots of COS-7 cells treatment with MG-132, TPEN and Z-VAD-FMK. *$P < 0.05$ and **$P < 0.01$ (Student's *t*-tests). (D) COS-7 cells expressing ATN1-Q19 and -Q77 were treated with MG-132, Z-VAD-FMK and TPEN. The mF2 fragment (black arrow) of ATN1-Q77 showed selectively increased reactivity after treatment with Z-VAD-FMK. (E) Twenty-four hours after treatment with Z-VAD-FMK and control dimethyl sulfoxide, COS-7 cells expressing ATN1-Q19 were visualized by immunofluorescence using His-tag (green) and C580R (red) antibodies. Immunocytochemistry showed that cytoplasmic aggregates of ATN1 C-terminal fragments were increased by Z-VAD-FMK treatment. Note that additional aggregates are labelled with C580R (red) in the cytoplasm of COS-7 cells with Z-VAD-FMK treatment (white arrows). The black arrowhead shows the nucleus. Scale bar = 10 μm.

nuclear accumulation of ATN1 and its cleaved fragments with polyQ expansion [17,24]. The details of the proteolytic processing of ATN1 remain unknown, whereas proteolysis of HD gene products (huntingtin) at the caspase-6 cleavage site was suggested to represent an initial event in the pathogenesis of HD [25]. In the present study, we aimed to elucidate some of details of the proteolytic processing of ATN1 and the mechanisms of ATN1 accumulation with the expansion of polyQ. We generated a cellular model of DRPLA, in which ATN1 and its fragments were accumulated in COS-7 cells expressing the *ATN1* gene by systematically increasing the number of polyQs expressed. We identified novel C-terminal fragments containing the polyQ tract in COS-7 and Neuro2a cells. ATN1 was processed into two C-terminal fragments that lost the nuclear localizing signal (NLS) in the N-terminal. One of the C-terminal fragments, F2, contained a polyQ tract; in addition, the mutant C-terminal fragment with an expanded polyQ tract (mF2) was specifically demonstrated in brain tissues from DRPLA patients. The increased amount of mF2 was likely caused by the pathological accumulation of ATN1, and was a result of the expansion of the polyQ tract. The present immunocytochemical study revealed that the accumulation of ATN1 and C-terminal fragments was localized in the cytoplasm and in the nucleus of cells. Indeed, the significant neuropathological features characterizing DRPLA are cytoplasmic inclusions, which are immunoreactive to ubiquitin and ATN1 antibodies, and also include nuclear inclusions in the DRPLA brains [2,26]. In the present study, the ATN1 antibody L55-2 labelled neuronal cytoplasmic and nuclear inclusions in the DRPLA brain. The biochemical examination of subcellular localization demonstrated that mF2 was preferentially localized in the cytoplasmic membrane/organelle and insoluble fractions, whereas the full-length ATN1 and the other C-terminal fragment were individually localized in the other fractions. Therefore, the proteolytic processing of ATN1 is likely to regulate the localization of C-terminal fragments. Moreover, a pan-caspase inhibitor selectively increased the accumulation of the C-terminal fragment in the cytoplasm, which recapitulated the cytoplasmic inclusion seen in the DRPLA brain. Taken together, these data suggest that the C-terminal fragment of ATN1 plays an important role in the accumulation of ATN1, ultimately leading to neurodegeneration in DRPLA.

Proteolytic processing of the gene products responsible for polyQ diseases has been shown to create toxic fragments containing expanded polyQ tracts *in vitro*, although whether all of the proteins undergo cleavage

in vivo is unclear. Previous studies have determined that caspase acts as a catabolic enzyme that targets proteins with a polyQ tract. For example, Wellington *et al.* [20] predicted that cleavage sites for caspase were contained in huntingtin, ATN1, ataxin-3 and androgen receptor, and showed that the cleavage of all four proteins could be inhibited by treatment of caspase inhibitors. Other studies have shown that, in HD, the N-terminal huntingtin fragment that contains the polyQ tract was cleaved by caspase-3 *in vitro* and in the human brain tissues [27], and that cleavage at the caspase-6 site in huntingtin was essential for the HD-related behavioural and neuropathological features in the YAC128 model of HD [25]. Previous studies of DRPLA also showed that caspase-3 generated a C-terminal fragment containing the polyQ by cleavage at Asp109 *in vitro*, and that blocking the cleavage at Asp109 reduced aggregation of mutant ATN1 with expanded polyQ in 293T cells [19,21]. In the present study, however, we demonstrated that an inhibitor of caspase-3 activity produced no reduction in the accumulation of C-terminal F2 fragment. Interestingly, the general caspase inhibitor Z-VAD-FMK increased the accumulation of the C-terminal F2 fragment in the cellular model of DRPLA. Caspases, a family of cysteine proteases, are mostly activated in the cytoplasm. Recent findings suggest that caspases may have other roles beyond their apparent role in apoptosis, including cell differentiation, proliferation and other nonlethal events [28]. The importance of activated caspases has also been extended to the central nervous system, where proteases have been shown to contribute to axon guidance, synaptic plasticity and neuroprotection [29]. A recent study demonstrated that caspase-3 directly cleaved AMPA receptor subunit GluR1 and modulated neuronal excitability [30]. We speculate that the cleavage of ATN1 by caspases may be involved in the regulatory mechanism of ATN1. In particular, decelerated cleavage of ATN1 might induce disruption of signal transduction and consequently cause neurodegeneration. Further investigations are necessary to determine the specific type of caspases that process ATN1 and the role of caspases in ATN1 accumulation.

Previous immunohistochemical studies demonstrated that ATN1 localized in both the nucleus and cytoplasm of neurones in the human central nervous system [15,22,31]. The data obtained from the biochemical and immunocytochemical analyses of the present study demonstrated that the full-length ATN1 and C-terminal fragments localized in the nucleus and the cytoplasm in COS-7 cells. The sequence of ATN1 contains an NLS in the N-terminal and a nuclear

export signal in the C-terminal. Mutational assays demonstrated that these signals are functional in ATN1 and that deletion or mutation of the nuclear export signal in ATN1 changed its localization, whereby it accumulated in the nucleus and increased cellular toxicity [18]. The cleavage products F1 and F2 of ATN1 represent a failure of the N-terminal NLS to import the proteins into the nucleus. Thus, we predict that the complete, full-length ATN1 is imported into the nucleus and is subsequently cleaved into F1 and F2 (Fig. 7A). There is also evidence that F1 and F2 are processed individually in the nucleus (Fig. S5A). TPEN, which suppressed the degradation of F1, failed to induce a change in F2 accumulation. Conversely, the inhibition of the F2 degradation by Z-VAD-FMK failed to induce the accumulation of F1. Thus, we expect that the C-terminal fragments of ATN1 are processed via independent pathways (Fig. 7A). Moreover, a biochemical examination of the intracellular distribution of the C-terminal fragments demonstrated that the localization of F2 differed from that of F1. We assume that F2 is again exported to the cytoplasm as a nucleocytoplasmic shuttling protein and functions in the cytoplasm, whereas F1 stays in the nucleus and executes its function on the nuclear matrix. As previously demonstrated in the human DRPLA brain tissue [15], ATN1 assembles in the perinuclear cytoplasm where caspases can be activated to regulate the accumulation of the F2 fragment. Thus, the shuttling system of ATN1 may play an important role in DRPLA

neurodegeneration. It is tempting to speculate that blocking caspase activity may also inhibit the shuttling system of ATN1, resulting in cytoplasmic accumulation of the ATN1 fragment and nuclear depletion of ATN1s (Fig. 7B).

The cellular models of DRPLA that were generated in the present study proved useful for further elucidation of the mechanisms of DRPLA neurodegeneration. Our models reproduced the pathological accumulation of the C-terminal fragment also observed in the DRPLA brain tissue. Moreover, the models demonstrated that the proteolytic processing of ATN1 regulated the intracellular localization of the cleaved fragments. Because the COS-7 and Neuro2a cellular models are able to demonstrate the accumulation of ATN1s in a much shorter period than that of DRPLA patient neuropathology, they are useful for analyzing the early stages of ATN1 accumulation with polyQ expansion. Using the cellular models, further experiments should be performed to reveal additional clues allowing exploration of a therapeutic target for neurodegeneration in DRPLA.

Experimental procedures

Construction of human ATN1 expression vector

The gene coding the full-length *ATN1* was amplified from Human Brain, cerebral cortex Marathon-Ready cDNA (Clontech, Palo Alto, CA, USA) with high-fidelity enzyme
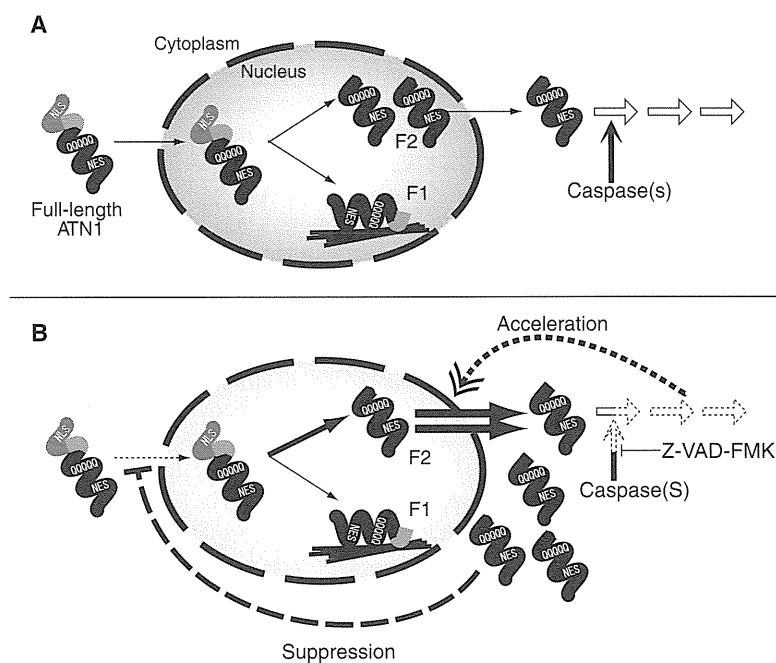
Fig. 7. (A) A schematic representation of a hypothetical model for proteolytic pathways of ATN1 in COS-7 cells. After importation into the nucleus, the full-length ATN is independently cleaved to F1 and F2 fragments. F1 stays within the nuclear matrix. F2 exports to the cytoplasm and assembles in the cytoplasmic organelle. Caspases are directly involved in the cleavage of F2, and regulate the accumulation of F2 in the cytoplasm. (B) When caspase activity is blocked by Z-VAD-FMK, the degradation of F2 is inhibited. This accelerates the accumulation of F2 in the cytoplasm and suppresses the nuclear transport of the full-length ATN1, which leads to the depletion of ATN1 and the fragments in the nucleus.

PrimeSTAR HS DNA polymerase (Takara Bio, Shiga, Japan) using the sequence specific primer by PCR and the product was cloned into pT7Blue (Novagen, San Diego, CA, USA). The resultant plasmid was designated as *ATN1*-pT7Blue. An *Xho*I restriction enzyme site was appended to Human *ATN1* at the 5′-end by PCR and changed vector to pRSETb (Invitrogen, Carlsbad, CA, USA) to yield a construct (*ATN1*-pRSET) in which the entire coding region of the gene is fused to a 6xHis-tag and a T7-tag at the 5′-region. To fuse a *Strep*-tag II sequence to the 3′-region of the *ATN1* gene, PCR was performed using the set of primers: forward, 5′-ATCGCAACCATCCATTCTACGTG-3′ and reverse, 5′-TTA<u>TTTTTCGAACTGCGGGTGGCTCC</u>AAGCGCTCAGTGGCTTGTCGCTTTCCTTCTTCAGGTG-3′ (the *Strep*-tag II sequence is underlined) and with *ATN1*-pT7Blue as the template. The PCR product was digested with *Bsp*1407I and *Eco*RI, which was ligated with the product of *ATN1*-pRSET digestion by the same set of enzymes. The resultant plasmid was designated as *ATN1-St*-pRSET. Furthermore, for effective expression of fusion ATN1, expression vectors were changed to pcDNA3.1(+) (Invitrogen) and pET-30a(+) (Novagen) from pRSET. A *Hind*III restriction enzyme site was added *ATN1* on *ATN1-St*-pRSET at the 5′-end by PCR. The *ATN1* fragment containing the three tag sequences was cleaved from *ATN1-St*-pRSET, and then ligated into pcDNA3.1(+) or pET-30a(+) vectors. The expression vectors were termed *ATN1*-pcDNA3.1 and *ATN1*-pET30. All recombinant plasmids were introduced into *E. coli* JM109. The nucleotide sequences of all constructs were confirmed using dye terminator methods.

Transient expression of ATN1 in COS-7 and Neuro2a cells

COS-7 and Neuro2a cells were maintained in DMEM supplemented with 10% fetal calf serum. FuGENE 6 (Roche Diagnostics, Basel, Switzerland) was used for the introduction of exogenous DNA into COS-7 and Neuro2a cells in accordance with the manufacturer's instructions. Briefly, 1×10^5 cells were plated on 35 mm dishes and, 24 h later, each dish was transfected with 2 μg of *ATN1*-pcDNA3.1, 0.02 μg *EmGFP*-pcDNA3.1 and 6 μL of FuGENE6, and incubated at 37 °C for 48 h. Whole cell lysates were prepared with 20 mM HEPES-buffered saline (pH 7.4), 1% SDS (HBS-SDS) with protease inhibitors. To determine the molecular basis for increasing the amount of ATN1, the stability of ATN1-Q19 or -Q77 was examined by inhibition of protein synthesis. Forty-eight hours after transfection, the COS-7 cells were incubated with cycloheximide (100 μg·mL^{-1}; Sigma-Aldrich, St. Louis, MO, USA). Cycloheximide interacts with the translocase enzyme and blocks protein synthesis in eukaryotic cells. The cells were then lysed after 0, 0.5, 1 or 2 h in HBS-SDS.

Subcellular protein extraction of COS-7 cells

Subcellular fractionation of COS-7 cells expressing ATN1s was performed using a ProteoExtract subcellular proteome extraction kit (Merck, Darmstadt, Germany) accordance with the manufacturer's instructions. Briefly, COS-7 cells (5×10^5 cells per 100 mm dish) were transfected with 10 μg of *ATN1-Q19-* or *-Q77*-pcDNA3.1, 0.1 μg of *EmGFP*-pcDNA3.1 and 27 μL of FuGENE6, and incubated at 37 °C for 48 h. After washing twice with ice-cold wash buffer, the cells were incubated with 1 mL of extraction buffer I at 4 °C for 10 min, and the supernatant was collected and used as the cytosolic fraction. The pellet was incubated with 1 mL of extraction buffer II at 4 °C for 30 min, and the supernatant was collected and used as the cytoplasmic membrane/organelle fraction. The pellet was incubated with 0.5 mL of extraction buffer III at 4 °C for 10 min, then the supernatant was used as the nuclear fraction, and the precipitate as the insoluble fraction.

Treatment with protease inhibitors

Twenty-four hours after transfection with *ATN1-Q19*-pcDNA3.1, the medium was replaced with serum-free medium, and then the cells were incubated with proteasome or protease inhibitors for 24 h. Cells were incubated with an equivalent amount of the vehicle, dimethyl sulfoxide as a control. The cells were treated with the proteasome inhibitors MG-132 (10 μM; Peptide Institute, Osaka, Japan), lactacystin (50 μM; Peptide Institute), calpain/proteasome inhibitor ALLN (0.2 μM and 20 μM; Roche Diagnostics), pan caspase inhibitor Z-VAD-FMK (50 μM; Peptide Institute), caspase-1 and -4 inhibitor Z-YVAD-FMK (50 μM; Bachem, Dübendorf, Switzerland), caspase-2 inhibitor Z-VDVAD-FMK (50 μM; BioVision, Mountain View, CA, USA), caspase-3, -6, -7 and -10 inhibitor Z-DEVD-FMK (50 μM; R&D Systems, Minneapolis, MN, USA), intracellular zinc chelator TPEN (0.5 μM; Sigma-Aldrich), intracellular calcium chelator EGTA-AM (50 μM; ABD Bioquest, Sunnyvale, CA, USA) and a broad-spectrum matrix metalloproteinase inhibitor GM6001 (50 μM; Merck). The cells were then assessed by western blotting and immunocytochemistry.

Expression of recombinant ATN1 in *E. coli*

The *ATN1*-pET30 was transformed into *E. coli* Rosetta2 (DE3)pLysS (Novagen)-competent cells. The Rosetta2 (DE3)pLysS strain is a BL21 derivative designed to alleviate codon bias when expressing heterologous proteins in *E. coli*, which supplies tRNAs for seven rare codons (AGA, AGG, AUA, CUA, GGA, CCC and CGG). The transformed *E. coli* was incubated overnight in 5 mL of LB culture medium containing kanamycin (50 μg·mL^{-1}) and chloramphenicol (34 μg·mL^{-1}) at 37 °C. After the addition of an aliquot of 100 μL of culture to 10 mL of the LB

culture medium containing kanamycin, the culture was incubated at 37 °C until A_{600} of 0.6 was reached. Expression of the ATN1 protein was induced by the addition of isopropyl thio-β-D-galactoside to a final concentration of 1 mM and incubation for 3 h at 37 °C. Cells were harvested by centrifugation at 1500 *g* for 10 min. Cell lysates were subjected to western blotting.

Assessment of ATN1-tag fusion proteins

ATN1-tag fusion proteins expressed by the COS-7 and *E. coli* cells were detected by western blotting using a *Strep*-tag II detection system. Samples (40 μg each) were electrophoresed in a 6% polyacrylamide gel. Proteins were transferred electrophoretically to a nitrocellulose membrane (GE Osmonics, Hopkins, MN, USA). The membranes were incubated in 5% BSA in NaCl/Tris (TBS) (pH 7.4). Then the membranes were incubated with Biotin Blocking Buffer (IBA, Göttingen, Germany) for 10 min, and *Strep*-tag II on ATN1 was visualized directly using *Strep*-Tactin HRP conjugate (dilution 1 : 5000; IBA) using an enhanced chemiluminescence reagent (ECL Plus; GE Healthcare, Little Chalfont, UK).

ATN1 antibodies

L55-2 is a polyclonal antibody raised against human ATN1. A synthetic peptide corresponding to human ATN1 residues 422-440 (NQPPKYTQPSLPSQAVWSQ) was conjugated with keyhole limpet hemocyanin and used to immunize rabbits. The antisera were purified by affinity chromatography. The resulting polyclonal antibody, L55-2, was used for immunoreactive probing. C580R is a polyclonal antibody raised against the C-terminus of human ATN1. C580R was reproduced according to a method that generated C580, as described previously [15]. 1C2 (Chemicon, Temecula, CA, USA) is a monoclonal antibody that recognizes polyQ tracts.

Immunoblotting

Protein concentrations were measured by bicinchoninic acid protein assay (Thermo Fisher Scientific, Waltham, MA, USA). Samples were electrophoresed in 6% polyacrylamide gel. The proteins were transferred to poly(vinylidene difluoride) (Atto, Tokyo, Japan). The poly(vinylidene difluoride) membranes were incubated in 5% nonfat milk powder in TBS, then they were incubated with monoclonal or polyclonal primary antibodies, followed by HRP-conjugated secondary antibodies. The antibodies used were: C580R (dilution 1 : 10 000), L55-2 (dilution 1 : 20 000), 1C2 (dilution 1 : 20 000), β-tubulin I monoclonal (dilution 1 : 10 000; Sigma-Aldrich), GFP monoclonal (Living Colors A.v. JL-8) (dilution 1 : 10 000; Clontech), TFIID polyclonal (dilution 1 : 5000; Santa Cruz Biotechnology, Santa Cruz,

CA, USA), Histone H4 polyclonal (dilution 1 : 200; Cell Signaling Technology, Beverly, MA, USA), HSP70 monoclonal (dilution 1 : 5000; StressMarq Biosciences, Victoria, BC, Canada) and vimentin clone VIM 13.2 monoclonal (dilution 1 : 5000; Sigma-Aldrich). Immunoreactive proteins were visualized using an ECL Plus.

Immunocytochemistry

COS-7 cells (5×10^4) were plated on 35 mm dishes and, 24 h later, each dish was transfected. Twenty-four hours after transfection, the cells were fixed with 4% paraformaldehyde, and then incubated with monoclonal GFP antibody (dilution 1 : 500; Chemicon) and polyclonal C580R antibody (dilution 1 : 200), as described previously [32]. Alexa 488 anti-mouse IgG or Cy3-labelled anti-rabbit IgG was used as secondary antibodies. Nuclei of cells were visualized by staining with 4′-6-diamidino-2-phenylindole.

Preparation of human brain tissue samples

Post-mortem brain tissue samples from four DRPLA patients, whose diseases had been diagnosed genetically by PCR analysis and confirmed pathologically, and the brain tissue samples from control subjects were examined [15,22]. Tissue samples (1.0 g) from the cerebra and cerebella were homogenized separately in five volumes of TBS with protease inhibitors (20 mM Tris–HCl, pH 7.5, 150 mM NaCl, 1 μg·mL^{-1} aprotinin, 1 mM EDTA, 10 μg·mL^{-1} leupeptin, 0.5 mM pefabloc SC and 10 μg·mL^{-1} pepstatin). In the crude subcellular fractionation experiment, the tissue samples (1.0 g) were homogenated in five volumes of 0.32 M sucrose/50 mM Tris–HCl (pH7.4), as described previously [15]. The homogenates were centrifuged at 1000 *g* for 20 min, and the pellet (nuclear fraction) was resuspended with TBS with protease inhibitors. Next, subcellular fractionation of ATN1 in the control and DRPLA brain tissues was analyzed by the ProteoExtract subcellular proteome extraction kit as described for the subcellular protein extraction of COS-7 cells. For immunohistochemical studies, the human control and DRPLA brain tissues were fixed in 10% formalin and embedded in paraffin. The sections from the brain tissues were immunostained with ATN1 antibodies as described previously [15]. The experiments involving human subjects were undertaken with the understanding and written informed consent of each individual. The NCGG Institutional Review Board approved the experiments involving human subjects.

Acknowledgements

157

References

1 Zoghbi HY & Orr HT (2000) Glutamine repeats and neurodegeneration. *Annu Rev Neurosci* **23**, 217–247.

2 Yazawa I (2003) Pathological mechanism of neurodegeneration in polyglutamine diseases. In *Recent Research Developments in Biophysics and Biochemistry*, Vol. 3 (Pandalai SG ed.), pp. 21–28. Research Signpost, India.

3 Orr HT & Zoghbi HY (2007) Trinucleotide repeat disorders. *Annu Rev Neurosci* **30**, 575–621.

4 Ross CA & Poirier MA (2004) Protein aggregation and neurodegenerative disease. *Nat Med* **10**(Suppl.), S10–S17.

5 Klement IA, Skinner PJ, Kaytor MD, Yi H, Hersch SM, Clark HB, Zoghbi HY & Orr HT (1988) Ataxin-1 nuclear localization and aggregation: role in polyglutamine-induced disease in SCA1 transgenic mice. *Cell* **95**, 41–53.

6 Saudou F, Finkbeiner S, Devys D & Greenberg ME (1998) Huntingtin acts in the nucleus to induce apoptosis but death does not correlate with the formation of intranuclear inclusions. *Cell* **95**, 55–66.

7 Kim M, Lee HS, LaForet G, McIntyre C, Martin EJ, Chang P, Kim TW, Williams M, Reddy PH, Tagle D *et al.* (1999) Mutant huntingtin expression in clonal striatal cells: dissociation of inclusion formation and neuronal survival by caspase inhibition. *J Neurosci* **19**, 964–973.

8 Arrasate M, Mitra S, Schweitzer ES, Segal MR & Finkbeiner S (2004) Inclusion body formation reduces levels of mutant huntingtin and the risk of neuronal death. *Nature* **431**, 805–810.

9 Ross CA (2002) Polyglutamine pathogenesis: emergence of unifying mechanisms for Huntington's disease and related disorders. *Neuron* **35**, 819–822.

10 Smith JK, Gonda VE & Malamud N (1958) Unusual form of cerebellar ataxia; combined dentato-rubral and pallido-Luysian degeneration. *Neurology* **8**, 205–209.

11 Naito H & Oyanagi S (1982) Familial myoclonus epilepsy and chroreoathetosis: hereditary dentatorubral-pallidoluysian atrophy. *Neurology* **32**, 798–807.

12 Takahashi H, Ohama E, Naito H, Takeda S, Nakashima S, Makifuchi T & Ikuta F (1988) Hereditary dentato-rubral-pallidoluysian atrophy: clinical and pathological variants in family. *Neurology* **38**, 1065–1070.

13 Sano A, Yamauchi N, Kakimoto Y, Komure O, Kawai J, Hazama F, Kuzume K, Sano N & Kondo I (1994) Anticipation in hereditary dentatorubral-pallidoluysian atrophy. *Hum Genet* **93**, 699–702.

14 Burke JR, Wingfield MS, Lewis KE, Roses AD, Lee JE, Hulette C, Pericak-Vance MA & Vance JM (1994) The Haw River syndrome: dentatorubropallidoluysian atrophy (DRPLA) in an African-American family. *Nat Genet* **7**, 521–524.

15 Yazawa I, Nukina N, Hashida H, Goto J, Yamada M & Kanazawa I (1995) Abnormal gene product identified in hereditary dentatorubral-pallidoluysian atrophy (DRPLA) brain. *Nat Genet* **10**, 3–4.

16 Igarashi S, Koide R, Shimohata T, Yamada M, Hayashi Y, Takano H, Date H, Oyake M, Sato T, Sato A *et al.* (1998) Suppression of aggregate formation and apoptosis by transglutaminase inhibitors in cells expressing truncated DRPLA protein with an expanded polyglutamine stretch. *Nat Genet* **18**, 111–117.

17 Schilling G, Wood JD, Duan K, Slunt HH, Gonzales V, Yamada M, Cooper JK, Margolis RL, Jenkins NA, Copeland NG *et al.* (1999) Nuclear accumulation of truncated atrophin-1 fragments in a transgenic mouse model of DRPLA. *Neuron* **24**, 275–286.

18 Nucifora FC Jr, Ellerby LM, Wellington CL, Wood JD, Herring WJ, Sawa A, Hayden MR, Dawson VL, Dawson TM & Ross CA (2003) Nuclear localization of a non-caspase truncation product of atrophin-1, with an expanded polyglutamine repeat, increases cellular toxicity. *J Biol Chem* **278**, 13047–13055.

19 Miyashita T, Okamura-Oho Y, Mito Y, Nagafuchi S & Yamada M (1997) Dentatorubral pallidoluysian atrophy (DRPLA) protein is cleaved by caspase-3 during apoptosis. *J Biol Chem* **272**, 29238–29242.

20 Wellington CL, Ellerby LM, Hackam AS, Margolis RL, Trifiro MA, Singaraja R, McCutcheon K, Salvesen GS, Propp SS, Bromm M *et al.* (1998) Caspase cleavage of gene products associated with triplet expansion disorders generates truncated fragments containing the polyglutamine tract. *J Biol Chem* **273**, 9158–9167.

21 Ellerby LM, Andrusiak RL, Wellington CL, Hackam AS, Propp SS, Wood JD, Sharp AH, Margolis RL, Ross CA, Salvesen GS *et al.* (1999) Cleavage of atrophin-1 at caspase site aspartic acid 109 modulates cytotoxicity. *J Biol Chem* **274**, 8730–8736.

22 Yazawa I, Hazeki N & Kanazawa I (1998) Expanded glutamine repeat enhances complex formation of dentatorubral-pallidoluysian atrophy (DRPLA) protein in human brains. *Biochem Biophys Res Commun* **250**, 22–26.

23 Knight SP, Richardson MM, Osmand AP, Stakkestad A & Potter NT (1997) Expression and distribution of the dentatorubral-pallidoluysian atrophy gene product (atrophin-1/drplap) in neuronal and non-neuronal tissues. *J Neurol Sci* **146**, 19–26.

24 Shimohata T, Nakajima T, Yamada M, Uchida C, Onodera O, Naruse S, Kimura T, Koide R, Nozaki K, Sano Y *et al.* (2000) Expanded polyglutamine stretches

interact with TAFII130, interfering with CREB-dependent transcription. *Nat Genet* **26**, 29–36.

25 Graham RK, Deng Y, Slow EJ, Haigh B, Bissada N, Lu G, Pearson J, Shehadeh J, Bertram L, Murphy Z *et al.* (2006) Cleavage at the caspase-6 site is required for neuronal dysfunction and degeneration due to mutant huntingtin. *Cell* **125**, 1179–1191.

26 Yazawa I, Nakase H & Kurisaki H (1999) Abnormal dentatorubral-pallidoluysian atrophy (DRPLA) protein complex is pathologically ubiquitinated in DRPLA brains. *Biochem Biophys Res Commun* **260**, 133–138.

27 Kim YJ, Yi Y, Sapp E, Wang Y, Cuiffo B, Kegel KB, Qin ZH, Aronin N & DiFiglia M (2001) Caspase 3-cleaved N-terminal fragments of wild-type and mutant huntingtin are present in normal and Huntington's disease brains, associate with membranes, and undergo calpain-dependent proteolysis. *Proc Natl Acad Sci USA* **98**, 12784–12789.

28 Lamkanfi M, Festjens N, Declercq W, Vanden Berghe T & Vandenabeele P (2007) Caspases in cell survival, proliferation and differentiation. *Cell Death Differ* **14**, 44–55.

29 McLaughlin B (2004) The kinder side of killer proteases: caspase activation contributes to neuroprotection and CNS remodeling. *Apoptosis* **9**, 111–121.

30 Lu C, Fu W, Selvesen GS & Mattson MP (2002) Direct cleavage of AMPA receptor subunit GluR1 and suppression of AMPA currents by caspase-3. *Neuromolecular Med* **1**, 69–79.

31 Yamada M, Tan CF, Inenaga C, Tsuji S & Takahashi H (2004) Sharing of polyglutamine localization by the neuronal nucleus and cytoplasm in CAG-repeat diseases. *Neuropathol Appl Neurobiol* **30**, 665–675.

32 Hashimoto N, Murase T, Kondo S, Okuda A & Inagawa-Ogashiwa M (2004) Muscle reconstitution by muscle satellite cell descendants with stem cell-like properties. *Development* **131**, 5481–5490.

Supporting information

The following supplementary material is available:

Fig. S1. Generation of an increased number of CAG repeats.

Fig. S2. Expression of ATN1-Q19 and -Q77 in COS-7 and Neuro2a cells.

Fig. S3. Intracellular distribution of ATN1 in COS-7 cells.

Fig. S4. TUNEL assay of mammalian cell expressed ATN1-Q19 and -Q77.

Fig. S5. Effect of other protease inhibitors on expressed full-length ATN1 and fragments in COS-7 cells.

This supplementary material can be found in the online version of this article.

Please note: As a service to our authors and readers, this journal provides supporting information supplied by the authors. Such materials are peer-reviewed and may be re-organized for online delivery, but are not copy-edited or typeset. Technical support issues arising from supporting information (other than missing files) should be addressed to the authors.
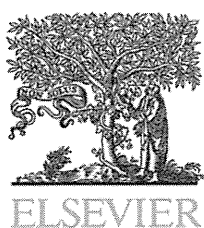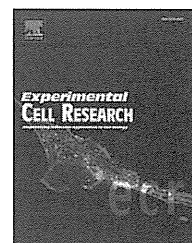
Research Article

Community effect triggers terminal differentiation of myogenic cells derived from muscle satellite cells by quenching Smad signaling

Michiko Yanagisawa[a,b,1], Atsushi Mukai[a,1], Kosuke Shiomi[a],
Si-Yong Song[c], Naohiro Hashimoto[a,*]

[a]Department of Regenerative Medicine, National Institute for Longevity Sciences, National Center for Geriatrics and Gerontology, 35 Gengo, Morioka, Oobu, Aichi 474-8522, Japan
[b]Aging Research, Nagoya University Graduate School of Medicine, 65 Tsurumai-cho, Showa-ku, Nagoya, Aichi 466-8550, Japan
[c]Institute of Neuroscience, Faculty of Pharmaceutical Sciences at Kagawa, Tokushima Bunri University, 1314-1 Shido, Sanuki-shi, Kagawa 769-2193, Japan

ARTICLE INFORMATION

ABSTRACT

A high concentration of bone morphogenetic proteins (BMPs) stimulates myogenic progenitor cells to undergo heterotopic osteogenic differentiation. However, the physiological role of the Smad signaling pathway during terminal muscle differentiation has not been resolved. We report here that Smad1/5/8 was phosphorylated and activated in undifferentiated growing mouse myogenic progenitor Ric10 cells without exposure to any exogenous BMPs. The amount of phosphorylated Smad1/5/8 was severely reduced during precocious myogenic differentiation under the high cell density culture condition even in growth medium supplemented with a high concentration of serum. Inhibition of the Smad signaling pathway by dorsomorphin, an inhibitor of Smad activation, or noggin, a specific antagonist of BMP, induced precocious terminal differentiation of myogenic progenitor cells in a cell density-dependent fashion even in growth medium. In addition, Smad1/5/8 was transiently activated in proliferating myogenic progenitor cells during muscle regeneration in rats. The present results indicate that the Smad signaling pathway is involved in a critical switch between growth and differentiation of myogenic progenitor cells both in vitro and in vivo. Furthermore, precocious cell density-dependent myogenic differentiation suggests that a community effect triggers the terminal muscle differentiation of myogenic cells by quenching the Smad signaling.

© 2010 Elsevier Inc. All rights reserved.

Introduction

Signaling molecules have both permissive and repressive effects on gene expression in the myotomes during embryonic myogenesis.

Skeletal muscle formation in the paraxial mesoderm is controlled by a number of signaling molecules emanating from neighboring tissues. Sonic hedgehog (Shh) and Wnt promote myogenesis [1]. In contrast, bone morphogenetic protein 4 (BMP4) inhibits premature differen-

tiation of the paraxial mesoderm. In addition, the negative action of BMP4 is counteracted by a specific BMP antagonist, noggin [1].

In contrast to embryonic skeletal muscle formation, the contribution of the signaling molecules to regulation of myogenesis during postnatal growth and repair of skeletal muscles remains to be determined. Skeletal muscle stem cells of adult muscle are known as muscle satellite cells that were characterized as a different class of myogenic cells from embryonic and fetal myoblasts [2]. Nonetheless, the signaling molecules that control embryonic and fetal myogenesis are likely to play a role in the regulation of growth and differentiation of muscle satellite cells and their descendant progenitor cells. Shh and Wnt have been reported to promote the proliferation of postnatal myogenic cells derived from muscle satellite cells [3–6]. It has been well established that BMPs induce heterotopic osteogenic terminal differentiation in myogenic cells derived from satellite cells [7–9]. Forced expression of constitutively active forms of BMP type I receptors and those of activin-like kinases (ALK) or receptor-regulated Smads (Smad1/5/8) induces ectopic osteogenesis in myogenic cells [10–13]. These results strongly suggest that the BMP–ALK–Smad signaling pathway renders the myogenic cell fate osteogenic. However, the concentration of exogenous BMPs required to induce osteogenesis in more than a half of myogenic cells is 100 ng/ml or higher [8,9,14,15] (Supplementary Fig. S1; Hashimoto, unpublished data). Recently, gene expression analyses of human skeletal muscle demonstrate that BMP4 is involved in the regulation of myogenic progenitor proliferation in human fetal skeletal muscle [16]. Co-Smad, Smad4, is involved in the inhibition of myogenesis but not the induction of osteogenesis, both of which are triggered by BMPs [15]. Therefore, these studies imply that the Smad signaling pathway plays a distinct role independently of heterotopic osteogenesis.

In vitro culture systems of myogenic cells have greatly contributed to elucidation of the molecular mechanisms underlying myogenic terminal differentiation of muscle satellite cells. Mouse and rat myoblast cell lines such as C2C12 [17], Ric10 [18], and L6 [19] from muscle satellite cells in postnatal muscle have been established and represent excellent cell culture models to analyze the proliferation and differentiation of myogenic progenitor cells. Terminal muscle differentiation of myoblastic cells is usually induced by reduction of the serum concentration in the culture medium. A number of studies have provided mechanistic insights into myogenesis using this differentiation-inducing condition because terminal muscle differentiation is synchronously induced in cells cultured in the serum-reduced differentiation medium. Nevertheless, we should keep in mind that the reduction of serum and/or growth factors would never be triggering mechanisms of terminal muscle differentiation in vivo. Another option to induce myogenesis of cultured myoblasts is high cell density culture. A number of muscle cell biologists may have had the common experience of myogenic cells beginning to undergo terminal muscle differentiation even in growth medium supplemented with a high concentration of serum when cultures become confluent. The spontaneous differentiation occurs asynchronously and focally in myoblast cultures under that growth condition. Thus, cell density-dependent and growth factor-independent induction of spontaneous myogenesis in vitro might be a unique model to investigate the initiation of myogenesis in regenerating muscles, which may contain large amounts of growth factors and cytokines. Mechanistic insights into spontaneous myogenesis may provide a new hypothesis concerning the molecular switch between growth and differentiation of myogenic cells during muscle regeneration.

In this study, we focused on the physiological role of the Smad signaling pathway in the switch between growth and differentiation of myogenic progenitor cells. Smad1/5/8 was activated in undifferentiated mouse myogenic Ric10 cells under growth conditions without the stimulus of exogenous BMPs. We show here that the community effect of myogenic cells quenches the Smad signaling pathway and triggers terminal muscle differentiation.

Materials and methods

Cell culture

The mouse myogenic cell line Ric10 was established from muscle satellite cells of the normal gastrocnemius muscle of an adult female ICR mouse [9,18,20]. Ric10 cells were plated on dishes coated with type I collagen (Sumilon, Tokyo, Japan) and cultured at 37 °C under 10% CO_2 in primary myocyte growth medium (pmGM) consisting of Dulbecco's modified Eagle's medium supplemented with 20% fetal bovine serum (FBS), 2% Ultroser G (Biosepra, Cedex-Saint-Christophe, France), and glucose (4.5 mg/ml) [9,14,21,22]. For induction of myogenic differentiation, the cells were plated and cultured for 24 h in pmGM, and then the medium was changed to primary myocyte differentiation medium (pmDM) consisting of the chemically defined medium TIS [23,24] supplemented with 2% FBS.

For micromass culture, dissociated single cells were cultured in pmGM at a density of 5×10^4 or 1×10^5 cells per 100-μl spot in a 35-mm dish or 5×10^2–2.5×10^4 cells per 50-μl spot in a well of a 24-well plate. After incubation for at least 2 h, pmGM was carefully added to each dish or well.

For inhibition of the Smad signaling pathway, Ric10 cells were cultured in medium supplemented with dorsomorphin (Calbiochem, Darmstadt, Germany) or recombinant mouse noggin and Fc of human IgG_1 chimeric protein (R&D Systems, Minneapolis, MN).

Promoter assay

Ric10 cells (2×10^4 per well in 12-well plates) were transfected with 0.75 μg of plasmids in the presence of 4.5 μl of FuGENE6 transfection reagent (Roche Diagnostic, Mannheim, Germany) as described [20,23–25]. A reporter plasmid MGN-luc was constructed by subcloning a 1.4 kb fragment of mouse myogenin promoter [26] (kindly provided by Y. Nabeshima) into pGL2 (Promega, Madison, WI). The transcriptional activity of Smad1/5/8 was determined using a BMP/Smad-dependent specific enhancer-containing reporter plasmid BRE-luc [27] (kindly provided by K. Miyazono). FLAG-tagged mouse Smad6 cDNA (kindly provided by K. Watanabe) and ALK2(KR) cDNA encoding a dominant negative form of human ALK2 (kindly provided by T. Imamura) were subcloned into pcDNA3 (Invitrogen, San Diego, CA). An expression plasmid for *Renilla* luciferase, pRL-TK (Promega) was co-transfected for normalization of transfection efficiency. A dual luciferase assay using a dual luciferase assay system was done essentially according to the manufacturer's instructions (Promega).

Induction of muscle regeneration by bupivacaine

Gastrocnemius muscles of Sprague–Dawley rats were injected with 500 μl of 0.5% bupivacaine hydrochloride (Marcain; Astellas Pharma, Tokyo, Japan) [28]. Three to four days after injection, the

gastrocnemius muscles were removed and quickly frozen in iso-pentane cooled with liquid nitrogen and processed for preparation of cryosections as described [29]. Muscle specimens were sectioned at a thickness of 8 μm with a cryostat.

Immunofluorescence analysis

The frozen sections and cultured cells were fixed with 4% parafor-maldehyde for 10 min at room temperature or on ice, respectively, and then incubated with primary antibodies. Primary antibodies included mouse monoclonal antibodies to mouse MyoD (1:10, Novocastra, Newcastle, UK), chicken sarcomeric myosin heavy chain (MHyC) (MF20, undiluted culture supernatant) [30], rat myogenin [31] (ascites, 1:1000, Developmental Studies Hybridoma Bank, Iowa City, IA), rabbit polyclonal antibodies to human phosphorylated Smad1/5/8 (pSmad) (1:100, Cell Signaling, Denver, CO), rat myogenin (1:200) [25], or mouse Id1 (1:100, affinity purified antibodies against β-galactosidase-mouse Id1 fusion protein) (Hashimoto, unpub-lished). Secondary antibodies included biotinylated or Cy3-labeled antibodies to mouse or rabbit immunoglobulin G (Jackson ImmunoR-esearch Laboratory, Bar Harbor, ME). The biotinylated antibodies were detected with streptavidin-conjugated Alexa488 (Jackson ImmunoResearch Laboratory). Cell nuclei were stained with 2,4-diamidino-2-phenylindole dihydrochloride n-hydrate (DAPI) (Sigma, St. Louis, MO). Samples were visualized using an upright microscope (model BX50; Olympus, Tokyo, Japan) and an inverted microscope (model IX71; Olympus) and a CCD camera (DP70; Olympus). Images were post processed using Adobe Photoshop (Adobe Systems, San Jose, CA). The signal intensity of pSmad in the nucleus was quantified using Image J software (NIH, Bethesda, MA). The signal density of pSmad in each sample was estimated from [signal intensity/nuclear area].

Immunoblotting

Sample preparation and immunoblot analysis were performed as described [24,25,32]. Immune complexes were detected by color-imetry with a BCIP/NBT detection kit (Nacalai, Kyoto, Japan) or an ECL kit (GE Healthcare, Piscataway, NJ). Primary antibodies included antibodies to MyHC, myogenin, Smad1 (Abcam, Cambridge, MA), pSmad, Id1 (Santa Cruz Biotech., Santa Cruz, CA) and flotilin-1 (Santa Cruz Biotech). Secondary antibodies included alkaline phosphatase (DAKO, Carpinteria, CA)- or horseradish peroxidase (GE Health-care)-labeled antibodies to mouse or rabbit immunoglobulin G. The PVDF membranes (Fluoro Trans W; Pall, Port Washington, NY) or X-ray films (Hyperfilm ECL; GE Healthcare) were scanned, and the signal intensity of each band was quantified using Image J software.

Results

Smad1/5/8 are phosphorylated in undifferentiated myogenic cells under growth conditions

To understand the physiological role of BMP–ALK–Smad signaling pathway during the growth and differentiation of postnatal myogenic cells, we detected phosphorylated Smad1/5/8 in the mouse myogenic progenitor cell line Ric10 with or without BMP2 stimulation. Smad1, Smad5, and Smad8 are functionally activated through their phosphor-ylation in a BMP–ALK–Smad axis-dependent manner [33]. The amount

of Smad1, a major Smad protein in Ric10 cells, remained constant even under BMP stimulation (Fig. 1A, upper panel). Exogenous BMP2 activated the Smad signaling pathway: although the amount of phosphorylated Smad1/5/8 in BMP-stimulated Ric10 cells was not more than 1.5 times that in unstimulated cells (Fig. 1A), exogenous BMP2 multiplied the transcriptional activity of Smad1/5/8 up to more than 10 times that in unstimulated cells (Fig. 1Ba). However, Smad1/5/8 was also phosphorylated in growing Ric10 cells without exposure to any exogenous ligand (Fig. 1A, left lane). Phosphorylated Smad1/5/8 was localized in nuclei of unstimulated, growing Ric10 cells (Fig. 1C). In addition, ALK2(KR), the dominant negative form of ALK2, significantly reduced the transcriptional activity of Smad1/5/8 in unstimulated cells (Fig. 1Bb). Exogenous BMP2 induced glycosylpho-sphatidylinositol-anchored alkaline phosphatase (ALP), an early marker of osteogenic differentiation through the activation of Smad signaling pathway in mouse myogenic cells (Supplementary Fig. S1) [9,14]. In contrast, the basal level activation of Smad1/5/8 didn't induce ALP expression in unstimulated mouse myogenic cells (data not shown) [9,14]. The results suggest that the Smad signaling pathway plays a physiological role that is independent of osteogenic differen-tiation in unstimulated, undifferentiated growing Ric10 cells.

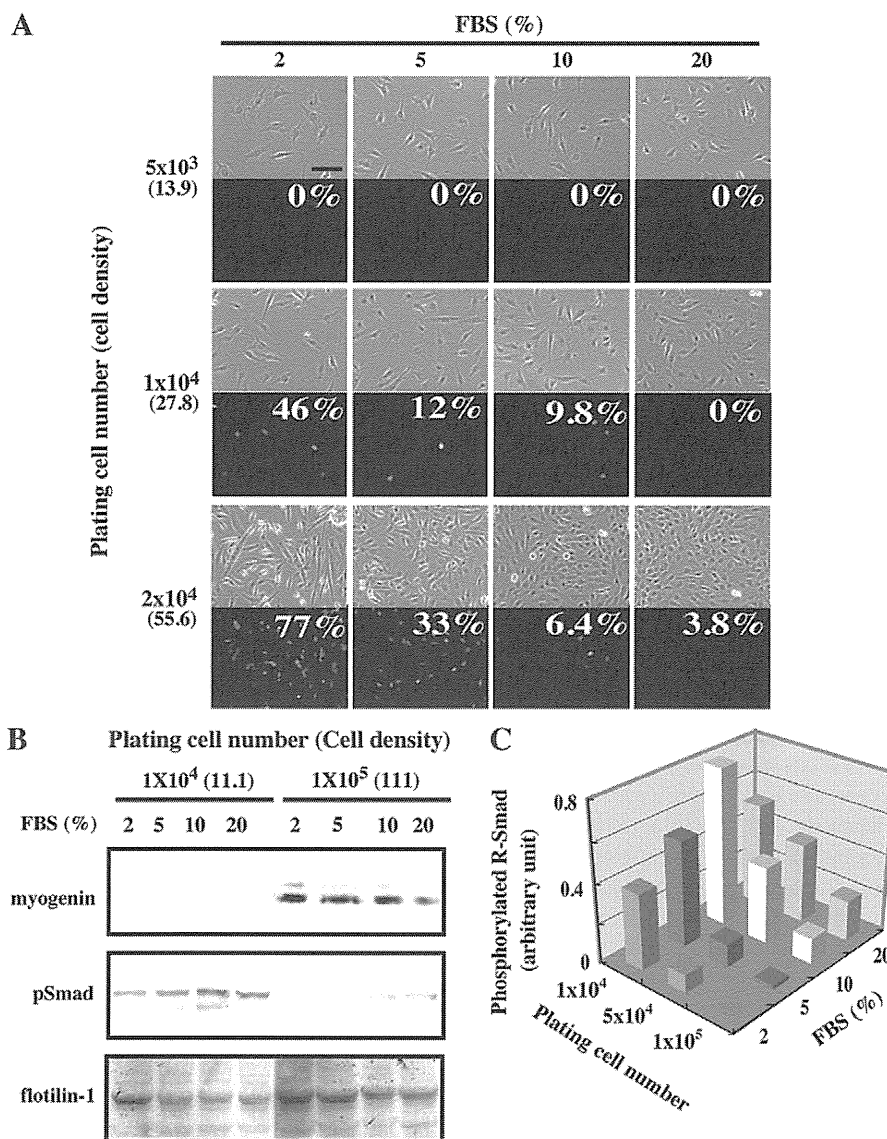### Myogenic terminal differentiation-inducing conditions reduce the amount of phosphorylated Smad1/5/8

Myogenic terminal differentiation of cultured myogenic cells depends highly on both the serum concentration in the medium and the cell density in the culture. Despite the low cell density, myogenic progenitor cells actually undergo myogenic differentiation in differ-entiation medium supplemented with a low concentration of serum. However, myogenic cells under the high cell density culture condition give rise to myotubes faster than those under the low cell density
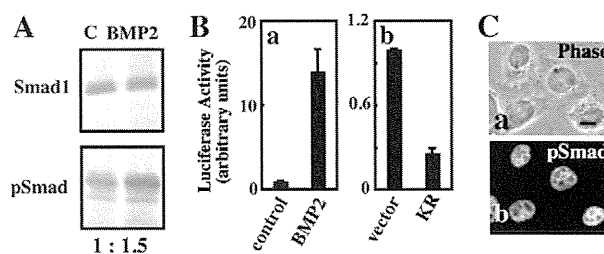
Fig. 1 – Phosphorylation of Smad1/5/8 in undifferentiated growing myogenic cells. (A) Total protein (20 mg) was prepared from Ric10 cells that had been cultured in pmGM supplemented with (lane BMP2) or without (lane C) BMP2 (100 ng/ml) for 24 h. Smad1 and phosphorylated Smad1/5/8 (pSmad) were detected on immunoblots. Relative amounts of pSmad are shown below the lower panel. (B) Ric10 cells were transfected with BRE-luc, Renilla luciferase-expression plasmid pRL-tk, and pcDNA3.1 (a and vector in b) or an expression plasmid for dominant negative ALK2 (KR). Then the cells were cultured in pmDM for 24 h and harvested for dual luciferase assay according to the manufacturer's instructions (Hashimoto and Ogashiwa, 1997). In (a), the cells were stimulated with BMP2 (100 ng/ml) or without (control) for 24 h. (C) Unstimulated, growing Ric10 cells showed nuclear localization of pSmad. The images were obtained by phase contrast (a) and epifluorescent (b) microscopy. Scale bar: 10 μm.

culture condition. To reveal the optimal culture condition for myogenic differentiation, different numbers of Ric10 cells were cultured for 24 h in the chemically defined differentiation medium TIS supplemented with different concentrations of serum. Actually, myogenic differentiation of Ric10 cells was exclusively induced under the culture condition with low serum and high cell density in an early period of culture (Fig. 2A). Then we determined the activation level of the Smad signaling pathway in Ric10 cells under different culture conditions. Smad1/5/8 was phosphorylated in low cell density culture (Fig. 2B,

lower panel). In contrast, the amount of phosphorylated Smad1/5/8 severely declined in the high cell density culture. The serum concentration in the medium also affected the phosphorylation level of Smad1/5/8 both in low and high cell density cultures. In addition, a low cell density in the culture and a high serum concentration in the medium synergistically activated the Smad signaling pathway (Fig. 2C). However, a low cell density in the culture more potently activated the Smad signaling pathway than a high serum concentration in the medium.

Fig. 2 – Down-regulation of Smad signaling pathway under myogenic differentiation-inducing conditions. (A) Ric10 cells were plated at a density of 5×10^3, 1×10^4, and 2×10^4 cells in a well of a 12-well culture plate and then cultured for 24 h in medium supplemented with different concentrations of fetal bovine serum (FBS). Cell density at seeding (cells per mm^2) is shown in parentheses left of the panels. Myogenin-positive nuclei were detected with a specific antibody and appeared as green dots. The percentage of myogenin-positive nuclei is shown inside the panels. Phase contrast and immunofluorescence images of the identical fields are shown as pairs. Scale bar: 100 μm. (B and C) Different numbers of Ric10 cells were plated in 35-mm dishes and cultured for 24 h in medium supplemented with different concentrations of FBS. Cell density at seeding (cells per mm^2) is shown in parentheses in (B). Myogenin, pSmad, and flotilin-1 were detected in 20 mg of total protein by immunoblotting analysis. Flotilin-1 was used as a loading control. Amounts of phosphorylated Smad1/5/8 on immunoblots were quantified and are represented as a three-dimensional graph (C).

The myogenic differentiation-specific transcription factor myogenin was expressed exclusively in the high cell density cultures of Ric10 cells, in which phosphorylation of Smad1/5/8 was down-regulated (Fig. 2B, upper panel). It should be noted that Ric10 cells undergo myogenic differentiation during prolonged culture (more than 48 h), even under the low cell density culture condition (Fig. 3A) [18]. Therefore, myogenic terminal differentiation was enhanced in the high cell density culture associated with inactivation of the Smad signaling pathway. The results suggest that the Smad signaling pathway is activated in undifferentiated proliferating cells and inactivated during the myogenic differentiation induced under the high cell density culture condition. The results imply the involvement of the Smad signaling pathway in a critical switch between growth and differentiation of myogenic cells.

Quenching of Smad signaling pathway is rate-limiting for myogenic differentiation induced by serum reduction

To determine whether the Smad signaling pathway is involved in the regulation of myogenic differentiation triggered by serum reduction, Ric10 cells were seeded at low (22 cells per mm^2) or high (111 cells per mm^2) cell density and then induced to differentiate in differentiation medium pmDM containing 2%

serum for up to 48 h. Ric10 cells seeded at high cell density gave rise to myotubes after 24 h under the serum-reduced culture condition whereas those under the low cell density culture condition began to fuse after 36 h (Fig. 3A). Expression of myogenin and a muscle differentiation marker MyHC was induced by serum reduction faster in the high cell density culture than the low cell density culture (Fig. 3B). In contrast to the muscle-specific proteins, the amount of a downstream factor of the Smad signaling pathway, Id1, declined faster in the high cell density culture than the low cell density culture. Serum reduction decreased the amount of phosphorylated Smad1/5/8 in both low and high cell density cultures. However, the phosphorylated Smad1/5/8 still remained under the serum-reduced, low cell density culture condition (Fig. 3B).

The previously mentioned results imply that quenching of the Smad signaling pathway is rate-limiting for myogenic differentiation induced by serum reduction. To explore this possibility, Ric10 cells were treated with the Smad signaling pathway inhibitor dorsomorphin [34]. Ric10 cells were seeded at low cell density (18 cells per mm^2) and then induced to differentiate in pmDM for up to 48 h. More than 90% of Ric10 cells underwent myogenic differentiation under this condition (Fig. 3A) [18]. Dorsomorphin further reduced the amount of remaining
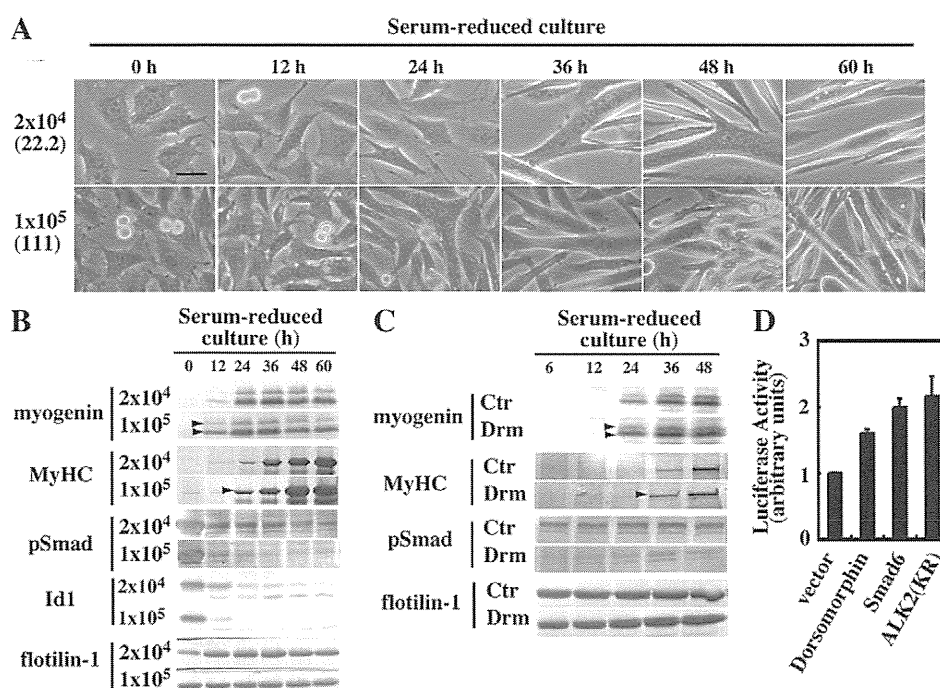
Fig. 3 – Activation levels of Smad signaling pathway during serum-reduced, low cell density culture. (A and B) Ric10 cells (2×10^4 cells per 35-mm dish; 22 cells per mm^2 for low cell density culture or 1×10^5 per 35-mm dish; 111 cells per mm^2 for high cell density culture) were plated and cultured in pmDM for up to 60 h. Images in (A) were obtained by phase contrast microscopy. Scale bar: 50 μm. Total cell lysates (20 μg of proteins) were subjected to immunoblotting analyses for MyHC, myogenin, pSmad, Id1, and flotilin-1 (B). Flotilin-1 was used as a loading control. Plating cell number is shown at the left of panels. Cell density at seeding (cells per mm^2) is shown in parentheses in (B). Arrowheads indicate the enhanced expression of MyHC and myogenin. (C) Ric10 cells (1×10^5 per 100-mm dish; 18 cells per mm^2) were cultured in pmDM with dorsomorphin (3 μM) or without (Control) for the indicated periods (h) shown at the top of panels. Total cell lysates (20 μg of proteins) were subjected to immunoblotting analyses for MyHC, myogenin, pSmad, and flotilin-1. Flotilin-1 was used as a loading control. Arrowheads indicate the enhanced expression of MyHC and myogenin in dorsomorphin-treated culture. (D) Ric10 cells were transfected with MGN-luc, pRL-tk, and pcDNA3.1 (vector and Dorsomorphin) or an expression plasmid for Smad6 or dominant negative ALK2 (ALK2(KR)). Then the cells were cultured in pmDM for 24 h and harvested for dual luciferase assay.

phosphorylated Smad1/5/8 (Fig. 3C). Expression of myogenin and MyHC was enhanced in Ric10 cells treated with dorsomorphin at 24 and 36 h of culture in pmDM. Taken together with the results, lowering the level of phosphorylated Smad may enhance myogenic differentiation triggered by serum reduction.

To determine whether the myogenic differentiation is negatively regulated through the activation of Smad1/5/8 under the serum-reduced culture condition, we determined the promoter activity of myogenin in Ric10 cells when the function of Smad1/5/8 was directly inhibited at distinct steps of the cellular signaling pathway: dorsomorphin inhibits phosphorylation of Smad1/5/8. Smad6, an inhibitory Smad, interrupts the interaction between Smad1/5/8 and Smad4 or BMP type I receptors [35,36]. ALK2(KR), the dominant negative form of ALK2, suppresses the activation of the BMP-receptor ALK2 [12]. Activity of the myogenin promoter in Ric10 cells during 24 h of differentiation culture was significantly enhanced by administration of dorsomorphin or expression of Smad6 or ALK2 (KR) (Fig. 3D). The results suggest that the quenching of Smad signaling pathway plays a role in the rate-determining step of terminal muscle differentiation triggered by serum reduction.

Concentration of phosphorylated Smad1/5/8 declines during myogenic differentiation in a cell density-dependent fashion

High cell density culture is another option for induction of myogenic differentiation in vitro. Ric10 cells were cultured in micromass to undergo myogenic differentiation independently of the serum concentration in the medium. When 5×10^4 or 1×10^5 Ric10 cells were seeded in a 100-µl spot, cells gave rise to a circular mass, the diameter of which was 6–8 mm (Fig. 4A). The cell density within a micromass declined along a central–peripheral axis. Myogenic terminal differentiation was induced exclusively in the central region of a cell mass during the 48 h after seeding, even when cells were cultured in growth medium pmGM containing 20% serum and supplementary growth factors (Fig. 4B). In the central region of the culture, the extremely high cell density was associated with a loss of phosphorylated Smad1/5/8 and the induction of myogenin expression even in pmGM (Fig. 4C). Myogenin expression was induced in a fraction of the nuclei in which the amount of phosphorylated Smad1/5/8 was severely reduced (Supplementary Fig. S2). In contrast, the cells retained phosphorylated Smad1/5/8 and did not express myogenin in the peripheral region with relatively low cell density. The results indicate that the Smad signaling pathway was inactivated under the high cell density culture condition, and also suggest that quenching of the Smad signaling pathway induces precocious myogenic differentiation even in the presence of growth factors.

Id1 gene is one of the target genes of the Smad signaling pathway [27]. Its gene product, Id1, inhibits transcription of the MyoD family and suppresses terminal myogenic differentiation [37]. Id1 expression was inhibited in Ric10 cells exclusively in the central region even in pmGM (Fig. 4D), although Id1 is normally expressed in a serum-dependent manner (Fig. 3B) [37]. Similar expression patterns of phosphorylated Smad1/5/8 and Id1 imply that inactivation of the Smad signaling pathway may induce myogenin expression and myogenesis through suppression of Id1 expression.

Furthermore, differentiation-inducing culture for 24 h in pmDM following 24 h of culture in pmGM triggered the robust
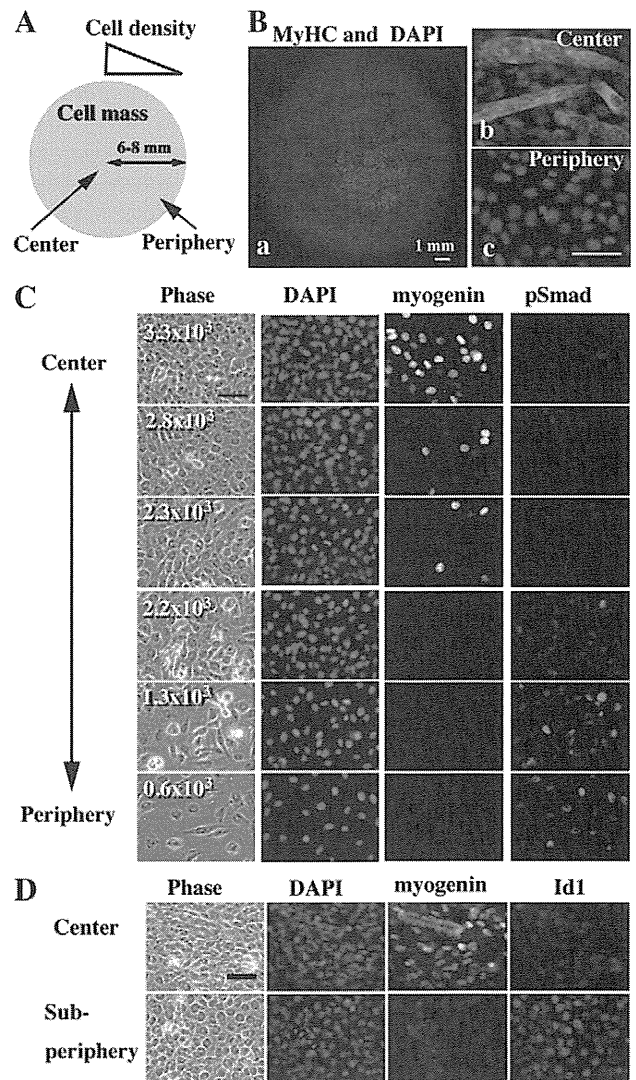
Fig. 4 – Down-regulation of phosphorylated Smad and Id1 during myogenesis triggered in high cell density culture. (A and B) For a micromass culture, 1×10^5 Ric10 cells were plated in a 100-µl spot and cultured in pmGM for up to 48 h. A diagram of micromass culture shows that cell density is reduced along with the center–periphery axis (A). MyHC was detected with a specific antibody (red) and nuclei were stained with DAPI (blue) in (B). Pictures show whole cell mass (a) and regions of center (b) or periphery (c). Scale bars, 1 mm (a) and 50 µm (b and c). (C and D) Ric10 cells (5×10^4 cells per 100-µl spot) were cultured in micromass for 48 h in pmGM. The cells were subjected to immunostaining with anti-myogenin and anti-pSmad or anti-Id1 antibodies. Nuclei were stained with DAPI. The numbers in phase contrast images in (C) represent the cell density of the indicated field (cells per mm^2). Images in each row were obtained from the same field. Scale bars: 50 µm.

expression of myogenin from the center to the sub-periphery of the cell mass (Fig. 5A). Ric10 cells gave rise to myotubes in the sub-peripheral region as well as the central region of the micromass. Serum reduction caused a rapid fall in the amount of phosphorylated Smad1/5/8 in micromass cultures (Fig. 5A). Id1 was down-